POLITECNICO DI TORINO

Master's Degree in Aerospace Engineering

Politecnico di Torino

Deutsches Zentrum für Luft- und Raumfahrt
German Aerospace Center

Master's Degree Thesis

Simulation of Thermoplastic Composite Storage Vessels for Cryogenic Fluids

Supervisors

Prof. Giacomo FRULLA

Dr. Ashley CHADWICK

Candidate

Dario Emanuele SALERNO

July 2025

Abstract

This thesis investigates the structural performance of composite materials with thermoplastic matrices for use in cylindrical tanks designed for liquid hydrogen storage under cryogenic conditions. A material property database at cryogenic temperatures is developed and implemented in ANSYS Workbench. The study systematically examines the influence of several design parameters, including composite wall thickness, matrix and fiber type, liner presence, and liner material. Among the materials evaluated, carbon fiber-reinforced PPS and PEEK exhibit the best performance, while glass fiber composites are less effective. While the incorporation of an HDPE liner reduces the IRF, greater reductions for a lower mass penalty are realised when using higher performance thermoplastics, particularly PEEK and PPS, as a liner material as well as composite matrix. The optimal configuration—a 7.2 mm linerless CFPPS tank—achieves the highest performance between the selected configurations. Although the modeling approach is intentionally simplified, the findings offer valuable insights for material selection and structural optimization. The study also identifies key areas for future work, including improved modeling fidelity and the exploration of additional materials and geometries.

Acknowledgements

I would like to express my sincere gratitude to the people and institutions that made this thesis possible.
I am profoundly grateful to the German Aerospace Center (DLR) for hosting me and providing an outstanding environment and the resources necessary for my study. A special and heartfelt thanks goes to my DLR supervisor, Ashley Chadwick, as his invaluable advice, consistent mentorship, and insightful discussions were instrumental in shaping this project. I would also like to thank all my colleagues at the DLR for their assistance and for creating a welcoming atmosphere that greatly contributed to my professional growth.
Finally, on a more personal note, I wish to express my heartfelt gratitude to my parents for their unconditional love and for always supporting me. My sincere thanks also go to my family and friends for being there for me, especially during the most challenging times.

Table of Contents

List of Tables

List of Figures

Acronyms

AFP
Automated Fiber Placement

ATL
Automated Tape Laying

CF
Carbon Fiber

COPV
Composite Over-Wrapped Pressure Vessels

CTE
Coefficient of Thermal Expansion

FEA
Finite Element Analysis

FW
Filament Winding

GC
Gravimetric Capacity

GF
Glass Fiber

HDPE
High-density polyethylene

IRF

Inverse Reserve Factor

LH2

Liquid hyrogen

LHV

Lower Heating Value

LM-PAEK

Low-Melt Polyaryletherketone

MLI

Multi layer insulation

PA6

Nylon 6

PEEK

Polyether Ether Ketone

PPS

Polyphenylene Sulfide

RVE

Representative volume element

VCS

Vapor Cooled Shield

Chapter 1

Introduction

As of now, it's estimated that 85% of the global energy system relies on fossil fuels, a finite resource projected to run out by the end of this century [21]. There are several key concerns here. One is the dependence on emerging countries, which can lead to fluctuations in the cost of fossil fuels. Another major issue is climate change and pollution, problems which are being partially addressed through the adoption of clean transportation fuels like hydrogen [9]. Hydrogen stands out as one of the most promising alternatives to fossil fuels, thanks to its unique properties. Firstly, it's the most abundant element on Earth and can be produced through various methods, some utilizing renewable energy sources, making hydrogen a completely sustainable energy source. Moreover, hydrogen doesn't produce any harmful particulates, making it the preferred fuel choice in the transportation industry, particularly within aviation, which aims to achieve zero carbon emissions by 2050 [10]. Despite its potential, hydrogen comes with inherent drawbacks. It is highly flammable and requires specific storage methods due to its low storage density. The storage density issue can be addressed by either storing hydrogen under high pressures, as commonly done in automotive applications using high-pressure composite over-wrapped pressure vessels (COPVs) [7], or in a liquid state at cryogenic temperatures below its boiling point (around 20K). The latter is more efficient than the compressed method, in fact while compressed gaseous hydrogen has a storage density ranging from 24.5 kg/m^3 to 41.4 kg/m^3 based on the operative pressure [31, 85, 88], liquid hydrogen can be stored at a density up to 70 kg/m^3 [72]. Although liquid hydrogen density is higher, integrating cryogenic tanks into aircraft requires certifiable and reliable storage systems. This work will investigate the structural performance of composite materials with thermoplastics matrices for use in cylindrical tanks designed for liquid hydrogen storage. Starting from the implementation of a material properties database into ANSYS Workbench, the influence of several design parameters such as composite wall thickness, matrix and fiber type, liner presence and material will be examined to find optimal configurations, laying a base for further analyses.

Chapter 2

State of the Art

2.1 Existing and Future Projects

Hydrogen finds application in a wide range of commercial uses, demonstrating its versatility and potential as a clean energy source. One of the main points of debate has always been its transportation. Nowadays, tanks are a well-defined technology and fully commercialized, making the storage and transport of hydrogen more feasible [10]. The automotive sector is at the forefront of hydrogen application, with several commercially available hydrogen-fueled vehicles. Notable examples include the Toyota Mirai, of which the hydrogen tank assembly is shown in Figure 2.1, and the Hyundai Nexo. Additionally, BMW is working on a hydrogen-fueled vehicle, although it remains to be clarified whether it will utilize liquid hydrogen.

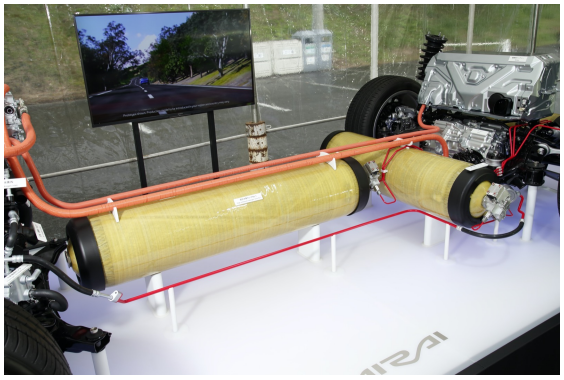

Figure 2.1: Close look of Toyota Mirai's hydrogen system [1]

Currently, automotive applications primarily use compressed storage for hydrogen. Despite advancements in vehicle technology, the fueling infrastructure remains an

open problem that hinders full-scale commercialization. The heavy-duty vehicle industry shows significant interest in hydrogen to bypass some cities' traffic limitations, indicating a potential area for growth. Moreover, the railway sector has expressed interest in hydrogen-fueled trains, particularly for use in areas where the lines are not or cannot be electrified. This would allow for the replacement of traditional diesel trains with cleaner hydrogen alternatives [45], as exemplified by Alstom's Coradia hydrogen train showin in Figure 2.2.

Figure 2.2: Coradia iLint [10]

In the early 2000s, Boeing successfully flew a small, unmanned aerial vehicle (UAV) powered by a hydrogen fuel cell, shown in Figure 2.3. This achievement illustrated the potential for hydrogen fuel cells to power future aircraft, offering a cleaner alternative to conventional fossil fuels [51]. Hydrogen remains a current research topic with future projects spearheaded by Airbus through their ZeroE initiative. Airbus is actively exploring hydrogen-powered aviation and has proposed three ZeroE concept aircraft: a turbofan, a turboprop, and a blended-wing body design, all aiming to reduce emissions and revolutionize the aviation industry [2].

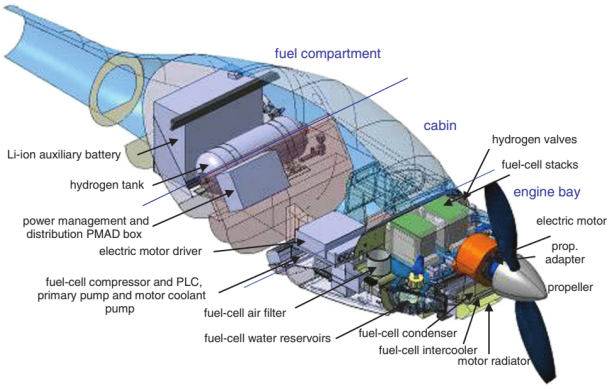

Figure 2.3: Boeing Fuel cell airplane demonstrator [51]

2.2 Hydrogen Storage

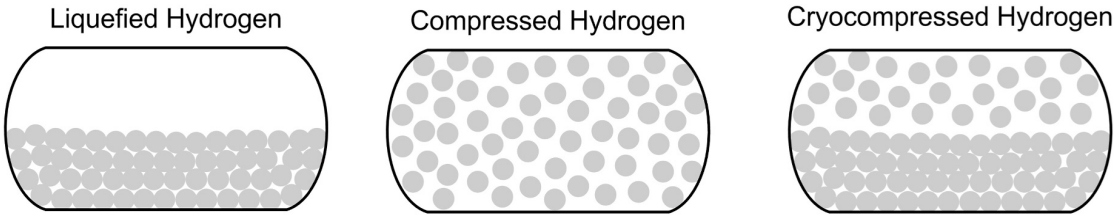

Figure 2.4: Hydrogen Storage Methods [81]

The energy content per unit mass of hydrogen, 120 MJ/kg of H2, makes it extremely attractive compared to other combustibles. However, this advantage comes with a great drawback, as hydrogen has the lowest volumetric energy density, owing to its low density at ambient temperature [27]. To make hydrogen viable and circumvent this problem, various storage methods have been developed and implemented, each based on a different concept, as shown in Figure 2.4. The different storage methods can be categorised in three main groups: compressed storage, cryogenic storage and material based storage. When considering transport applications, storage of hydrogen in another medium, be it chemical compound or porous material, incurs a prohibitive mass penalty and is therefore excluded from the scope of this work.

Compressed storage is one of the most widely used storage techniques. This method involves compressing hydrogen in gaseous state into cylinders, containers or even natural underground caves. The choice of storage depends on the specific application [31, 85, 88]. For transportation the choice falls on cylindrical vessels, into which hydrogen is stored under pressures that reach up to 700 bar. One of the advantages of compression storage is its technological simplicity, facilitating high rates of both filling and release. Unlike some other storage methods, compression storage requires no additional energy for release, streamlining the process. However this simplicity comes with a trade-off, as compression storage consumes approximately 13%-18% of the Lower Heating Value (LHV) of hydrogen, which renders it less economically viable. Furthermore, the volumetric density does not increase proportionally with the pressure, due to gaseous hydrogen following the real gas law. For instance, the volumetric density at 350 bar is 24.5 kg/m^3, while at 700 bar, it rises to 41.4 kg/m^3.

One notable concern associated with high-pressure vessels is the increased risk of explosion and safety hazards. Factors such as shocks and temperature gradients can exacerbate these risks, necessitating careful handling and maintenance protocols. Despite these challenges, compressed hydrogen storage remains widely used across various automotive applications, as the aforementioned Toyota Mirai.

Cryogenic storage represents another prominent method for storing hydrogen, offering distinct advantages over compression. Liquefied hydrogen, with its density of 70 kg/m^3, higher than compressed hydrogen, allows for greater energy storage per unit volume, translating to a higher volumetric energy density. This attribute makes liquefied storage an appealing option as its production technology stands is already well-established in the field, even though its application in transportation is still under development [81].

Moreover the higher density of liquid hydrogen and the ability of storing it at ambient pressure enables a reduction in vessel size and weight compared to the compressed gas, which needs stronger and bigger vessels to withstand high pressures. It is also shown how, thanks to its high volumetric energy density, liquid hydrogen powered aircraft are more advantageous than kerosene fueled ones, as the latter has a volumetric energy density of 43 MJ/kg [19]. One notable benefit of using liquid hydrogen is that it is less corrosive than when it is in its gaseous form, due to the lower mobility of hydrogen atoms at 20 K, hence using metal vessels becomes more viable as embrittlement is reduced [47]. Cryogenic storage is not without its drawbacks. The liquefaction process consumes approximately 30-40 percent of the lower heating value of hydrogen, rendering it costly [81, 88]. Additionally, a significant concern is the boil-off effect, wherein hydrogen is lost due to energy input from the surroundings, resulting in a vaporization-induced loss that ranges between 0.3 and 3 percent per day [48, 59]. This issue diminishes its effectiveness for automotive applications, despite its widespread utilization in space applications, as fuel for launchers, and a particular interest in the aviation field.

Cryo-compressed storage, combining elements of both compressed and cryogenic storage, has garnered attention within hydrogen storage research. This method involves storing hydrogen at cryogenic temperatures while maintaining a minimum pressure typically ranging from 250 to 350 bar. This hybridization offers several advantages, including higher densities and mitigation of the boil-off effect [6]. The resultant storage density can reach up to 87 kg/m^3 [6, 50, 81, 88]. Despite its clear advantage in terms of volumetric density, this technique proves to be quite resource-intensive, as it bears both the disadvantages of the compressed and cryogenic storage, for a small increase in volumetric density. Table 2.1 summarises the key differences between the aforementioned methods.

Table 2.1: Comparison of Hydrogen Storage Methods

Method	Compressed	Cryogenic	Cryo-Compressed
Storage State	Gas	Liquid	Dense, cold gas or liquid
Operating Pressure	350 - 700 bar	1-5 bar	350-500 bar
Operating Temperature	295 K	20 K	40-120 K
Volumetric Density	25 kg/m^3 (350 bar) - 40 kg/m^3 (700 bar)	70 kg/m^3	87 kg/m^3

2.3 Tank types

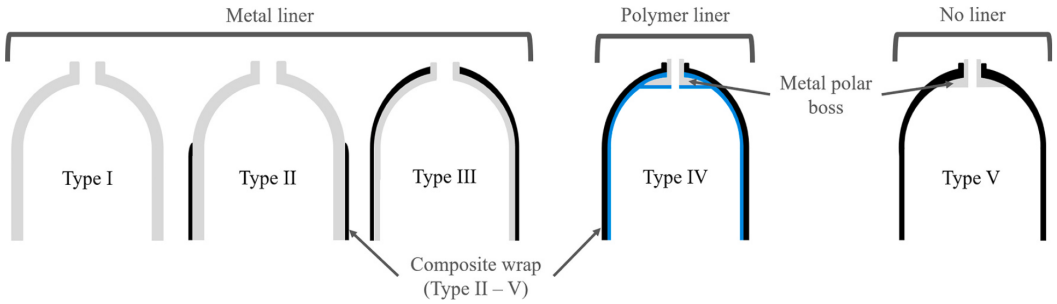

Figure 2.5: Schematics of the different types of tank material combinations and their designations [7]

In an attempt to reduce the mass and therefore increase the storage efficiency of tank structures, different material combinations have been explored, as shown in Figure 2.5. There are currently five types of tank with each one considered evolution of the previous design:

a. **Type I**: Made completely of metal, usually Stainless Steel or an Aluminium Alloy, Type I tanks are capable of withstanding pressure up to 30bar. As higher pressures lead to the need of a thicker metal wall, hence a significant increase in weight[14, 81].

b. **Type II**: It consists in a metallic core, wrapped with a composite layer, which allows to optimize weight but increasing costs.

c. **Type III**: Composed by a steel or aluminium liner, completely wrapped with composite, it's the first design that wants to move out of the full metal use as composites, especially carbon fibers, are stronger in tension than steel or aluminium, allowing higher pressures or thinner walls.

d. **Type IV**: The actual State of the Art, this tank type consists of a plastic liner, usually HDPE [22], wrapped completely with a composite material. This design moves away from the use of metal, solving some of the issues given by the hydrogen interaction with the metal components such as embrittlement.

e. **Type V**: Fully Composite tank, it does not have a liner. The absence of the liner eliminates the need of compatibility between liner and composite, factor that becomes relevant especially at cryogenic temperatures, due to the different behaviour of the composite wall and the plastic liner, although making other problems more relevant such as the permeability of hydrogen

through the composite, which in Type IV vessel can be reduced tanks to the liner properties. Furthermore the liner elimination leads to a weight reduction together with a better fatigue life [7, 8, 13].

This clear progression from all-metal to full composite linerless designs underscores the industry's drive towards composite materials. The primary motivation is the significant weight reduction and corresponding increase in gravimetric storage efficiency that composites offer over traditional metals. For demanding applications like aerospace and automotive, where minimizing mass is critical, advanced composite tanks, type IV and V are not just advantageous but essential.

Therefore, this work will focus on performance and design parameters of these composite vessels.

2.3.1 Tanks for the storage of liquid hydrogen

As one of the constraints of liquid hydrogen storage is to limit the thermal gradient between the liquid and the outer environment, three insulation techniques (Figure 2.6) are commonly utilised, consisting of a further element to take into account in the design of the tank.

The traditional method consists in a double-jacketed tanks system, where the outer jacket is filled with liquid nitrogen.

A more effective technique for cryogenic applications is vacuum insulation, where a vacuum between the inner and outer walls of the tank drastically reduces heat transfer from conduction and convection. This method is often enhanced by adding super insulation in the vacuum space, using either reflective powder or Multi-Layer Insulation (MLI). The latter limits every form of heat transfer by encasing the tank with layers of materials with very low thermal conductivities, in the range of 10 to 50 $\mu W/mK$ at temperatures between 20 and 300 K, within the high vacuum environment [59, 78].

At last, Vapor-Cooled shielded tanks (VCS), which are a modified design of the MLI tanks where the boil-off effect of hydrogen is predicted via the implementation of a vapor chamber in which the hydrogen vapors are collected and act as an additional insulating layer [74, 75].

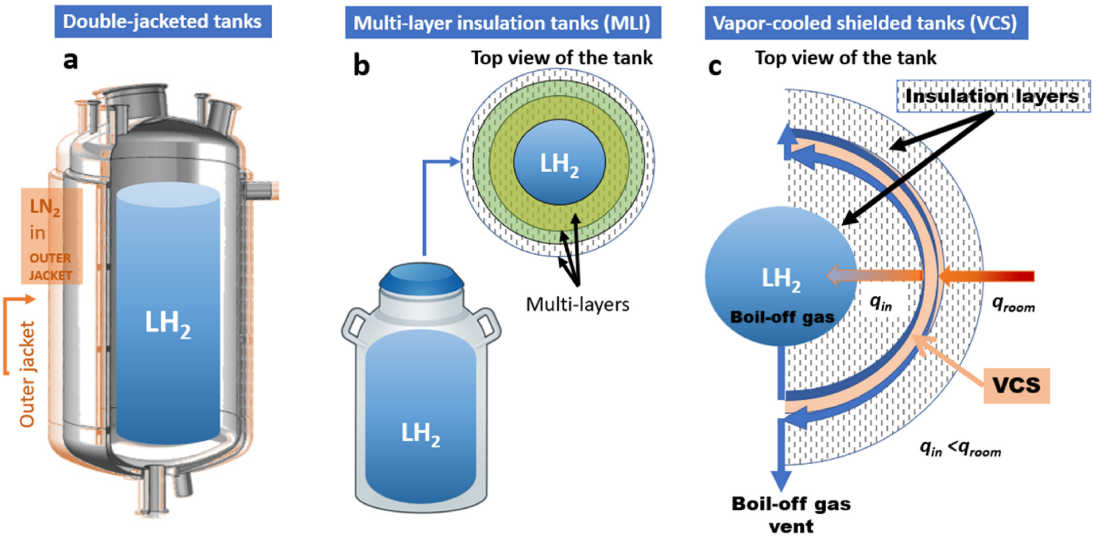

Figure 2.6: Overview of the different tank configurations for liquid hydrogen storage [59]

2.4 Tank Manufacturing

2.4.1 Manufacturing Methods

Due to the complex shape of tanks, particularly the end caps, manufacturing of type IV and V tanks typically utilises either winding, AFP, or braiding.

Filament Winding (FW) stands as a well-established technique in crafting composite cylindrical structures [52], such as rocket engine cases and launch tubes. This method involves an automated process for strategically positioning fibers in patterns that conform to stress pathways, thereby maximizing the efficient use of high-strength fibers and enhancing structural integrity [13]. The process is illustrated in Figure 2.7.

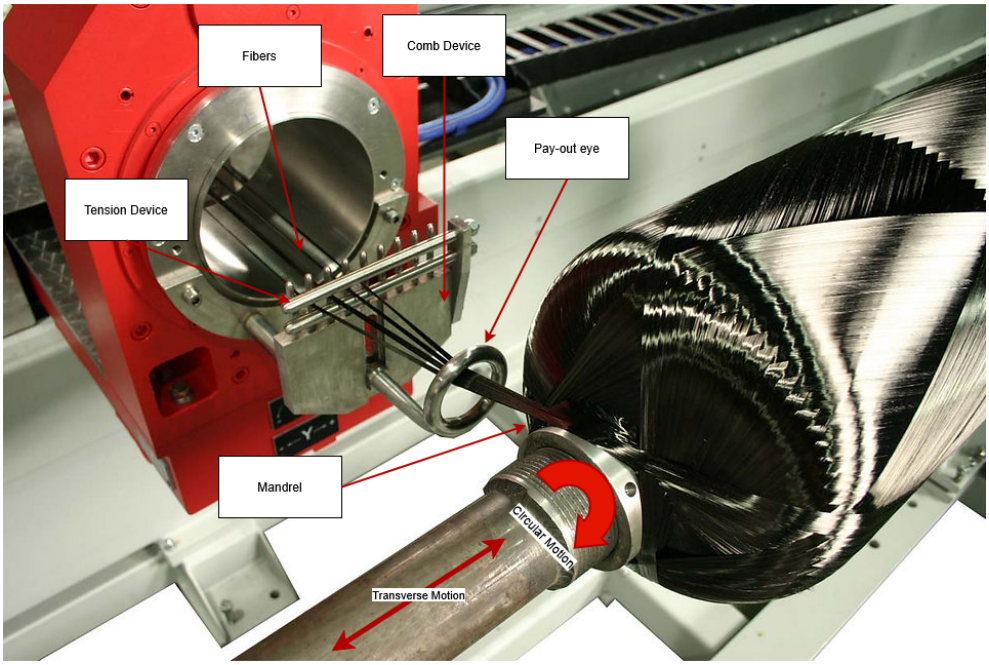

Figure 2.7: Close look of the FW process [68]

A widely used manufacturing technology that enables low-cost, high-efficiency production is Automated Fibre Placement (AFP) [66]. In this process pre-preg material is fed to a compaction roller, heated to its processing temperature (tack for thermosets and melt for thermoplastics), and consolidated onto a substrate to create a layered structure, as illustrated in Figure 2.8.

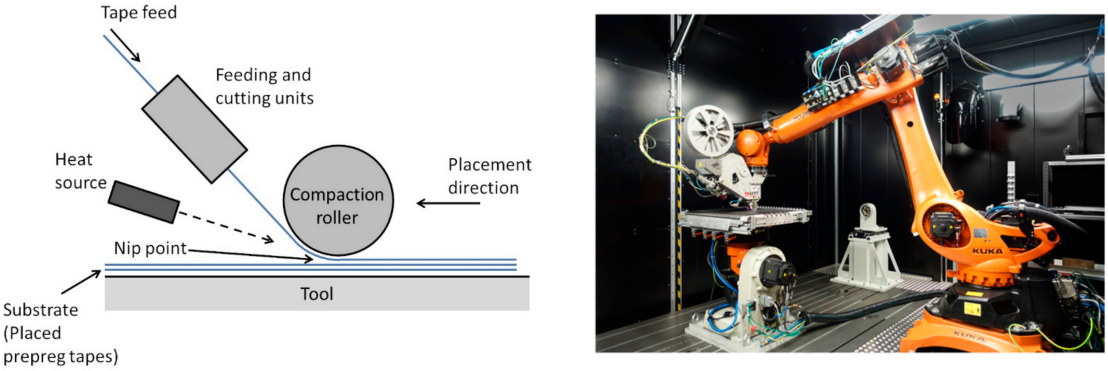

Figure 2.8: Schematics of the AFP process [7] (left), AFP facility at DLR in Stuttgart [60] (right)

Braiding stands out as an advanced method in textile manufacturing, utilized for crafting both two-dimensional and three-dimensional components. Unlike laminated structures, braids intertwine yarns to establish seamless connectivity between layers, thereby enhancing impact resistance, damage tolerance, and reinforcement through thickness. Yet, despite the array of advantages, braided composites present challenges due to their intricate fiber architecture, particularly in selecting appropriate strain measurement and characterization techniques [36, 57].

Figure 2.9: Braiding Tool Overview [52] (left), Cylindrical structure manufacture via braiding [3] (right)

2.4.2 Composite Materials used for Tanks

Composite materials have emerged as a preferred solution for tank structures due to their excellent strength-to-weight ratio, corrosion resistance, and fatigue durability. These inherent properties allow for the construction of lightweight, durable vessels capable of withstanding the high-pressure and temperature requirements typical of applications like hydrogen storage [62]. Furthermore, they present a cost-effective solution; their low weight and ease of fabrication reduce initial manufacturing costs, while their long service life and minimal maintenance requirements lower the overall lifetime cost of the vessel [62]. A key advantage of the technology is the ability to tailor material properties through different fiber and matrix combinations. For instance, specific strength and modulus targets can be achieved by varying reinforcement types and layup configurations, providing engineers with the design flexibility needed to optimize a vessel for a specific application [62].

The choice of matrix material plays a pivotal role in defining the overall behavior and manufacturability of composites. Thermoplastics are gaining prominence over traditional thermosets due to their recyclability, higher toughness, and ease of processing [35, 63]. In structural applications such as storage tanks, these materials also exhibit strong resistance to crack propagation and environmental degradation[61]. This robustness, combined with thermal resistance and reprocessability, makes thermoplastic composites highly suitable for applications demanding longevity and mechanical reliability [10].

Another critical factor in optimizing composite performance is the selection of the appropriate fiber material. Carbon fibers and their high-strength variants in particular, such as Toray T1000, are often preferred for their superior tensile properties, which support the vessel in withstanding high internal pressures and cyclic loads. However, lower-strength but more cost-effective fibers like Toray T300 or T700 may be suitable for weight-sensitive applications, or where moderate pressures are expected [62]. Glass fibers are taken into consideration in low-pressure applications given the lower cost compared to carbon fibers, circa 2 $/kg compared to the 20 $/kg of carbon, and tensile moduli comparable to low-strength carbon fibers like Toray 300, 90GPa for high modulus variants of glass fiber and 135 GPa for T300 [25]

In addition to matrix and fiber selection, composite performance can be further enhanced through nanomaterial integration. The inclusion of graphene within the matrix significantly improves mechanical stiffness and thermal conductivity, both of which are essential for high-performance storage applications [16]. These advanced composites promise superior durability and weight efficiency, aligning with the evolving demands of energy storage systems.

In specialized environments like cryogenic storage, one of the main challenges is the mismatch in the coefficient of thermal expansion (CTE) between the fiber

and the matrix. This mismatch can lead to residual stresses, microcracking, and a reduction in adhesion between fiber and matrix when the composite is subjected to large temperature changes from ambient to cryogenic conditions [79]. These microcracks can create pathways for leaks, compromising the safety and efficiency of cryogenic storage systems. Therefore, selecting matrix and fiber materials with compatible CTEs or developing matrix systems with improved toughness at low temperatures is crucial for mitigating these effects and ensuring the long-term reliability of composite tanks in cryogenic applications.

Matrix	**Fiber**	**Source**
DGEBA/TGMDA/DDS	Carbon	[79]
Epoxy	Toray T700 (Carbon)	[32]
Elium 591 (Arkema)	H2550-24K Carbon Fiber	[35]
Epoxy, Phenolic, Vinylester, Polyester	Carbon T700	[62]
Epoxy	Glass Fiber	[61]
PEEK, PA6, PPS; HDPE, PA (for liner)	Carbon	[10]

Table 2.2: Overview of materials investigated in the reviewed papers

Given these significant challenges, and because the storage temperature of liquid hydrogen is 20 K, it is necessary to further explicate the effect of cryogenic temperatures on the behaviour of composite materials.

2.5 Effects of cryogenic temperatures

It is necessary to understand how the composites behavior is influenced by low and cryogenic temperatures. An overview of material properties changes has been extracted from Sapi et al. [71] and is below elaborated upon.

Regarding Tensile behaviour, as temperatures drop, both the Young modulus and tensile strength of the matrix undergo significant increases. This phenomenon arises from the reduced mobility of polymer chains, which strengthens the molecular binding forces within the matrix. Consequently, the material stiffens as stress relaxation slows down at lower temperatures, with stress relaxation potentially ceasing entirely under cryogenic conditions, further bolstering stiffness [23, 26, 29, 38, 82].

The impact of cryogenic temperatures varies depending on the type of resin employed. Moreover, the inherently non-uniform molecular structure of fibers is a factor.

At cryogenic temperatures, fibers typically experience only slight improvements

in modulus. For instance, Carbon Fiber (CF) may develop surface cracks, diminishing its single fiber strength. However, this reduction is countered by the increased strength of the fiber-resin interface due to thermal expansion [87].

Significant enhancements are observed in the longitudinal Young modulus and tensile strength. Moreover, the transverse strength and stiffness of composite materials largely depend on resin and interface properties, exhibiting notable increases at cryogenic temperatures.

Decreases in longitudinal strength reported are attributed to internal stresses during cooldown from the cure temperature to cryogenic temperatures. Additionally, elongation at break diminishes as resin loses ductility, while stiffness increases. This effect is noticeable not only in single Carbon fibers but also in composite materials. Interestingly, Glass Fibers display a contrasting effect under cryogenic conditions. While cracks may form, they do not lead to failure but instead contribute to increased material density and act as stress relief mechanisms.

The internal mechanisms that influence the Tensile behaviour of the composites, act as well on Compression and Shear behavior. Under Compression, both the resins modulus and strength increase, and since the matrix bears the load during compression, its increased stiffness and stronger bond with fibers enhance the longitudinal compressive strength and stiffness of composite materials. This improved support also shifts failure from kinking to fracture at lower temperatures. The shear behavior of fiber-reinforced composites is primarily influenced by the matrix's characteristics. Similar to tension, at cold temperatures, the resin becomes stiffer, stronger, and less prone to strain before failure. This change is accompanied by the elimination of non-linearity in the shear stress-shear strain response as temperature decreases.

Thermal expansion significantly influences the mechanical characteristics of composites under cryogenic and low-temperature conditions.

The coefficient of thermal expansion (CTE) varies among fibers depending on their longitudinal and transverse orientations. Generally, aramid and most carbon fibers expand lengthwise during cooldown, while glass and basalt fibers contract in this direction. Conversely, in the transverse direction, aramid, glass, and basalt fibers contract, while carbon fibers expand. This interplay between fibers and resin creates a complex stress environment, leading to the development of compressive stresses at the fiber-resin interface. These stresses enhance interface strength, a critical factor contributing to the improved mechanical properties seen in composites at cryogenic temperatures.

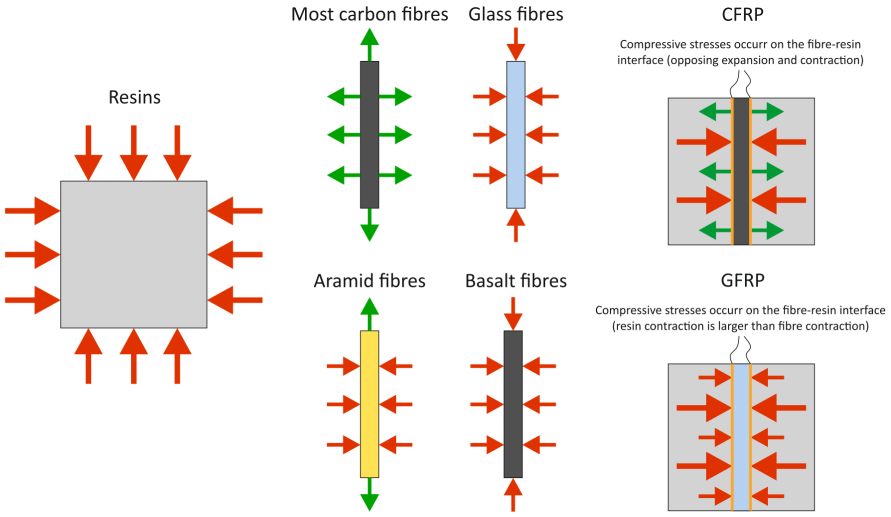

Figure 2.10: Deformation of materials during cooldown to CT [71]

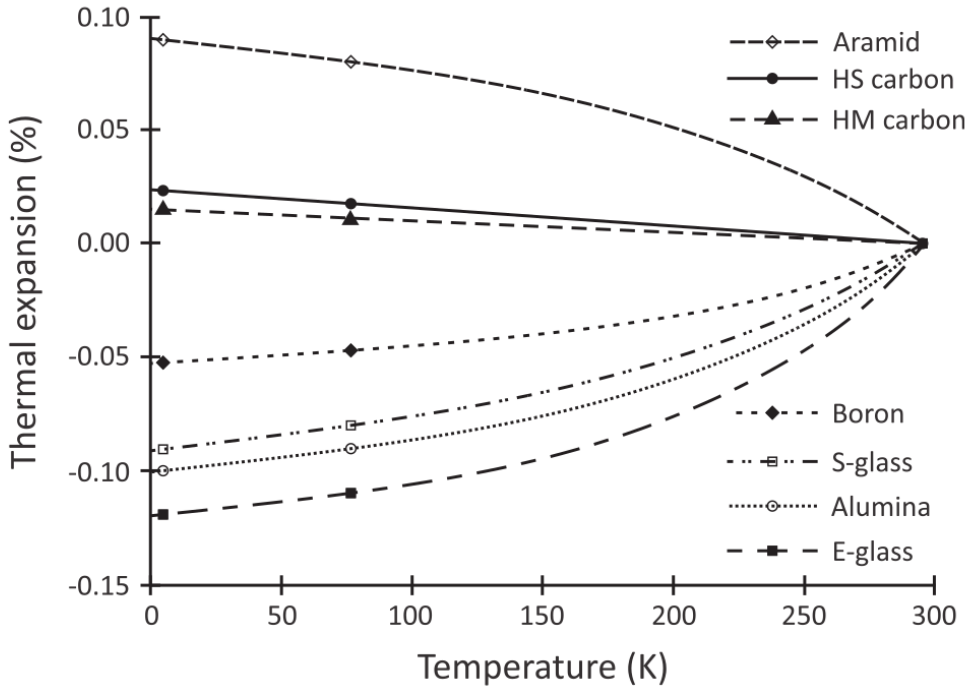

Figure 2.11: Thermal expansion of UD fiber-reinforced laminates [67]

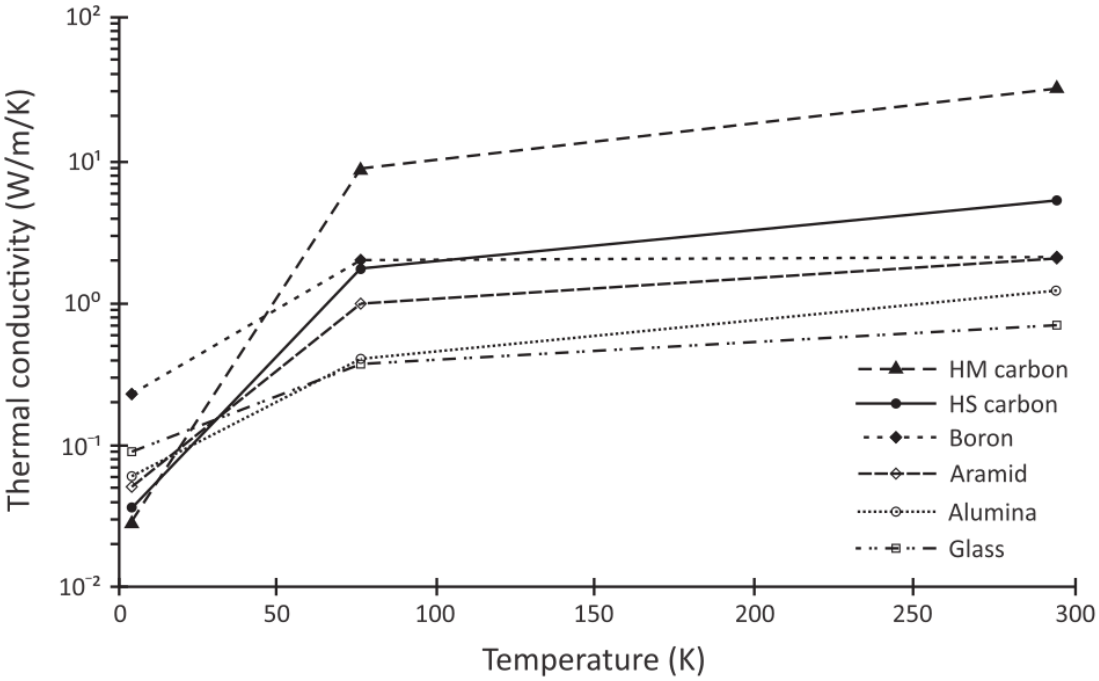

Figure 2.12: Thermal Conductivity of UD fiber-reinforce laminates [67]

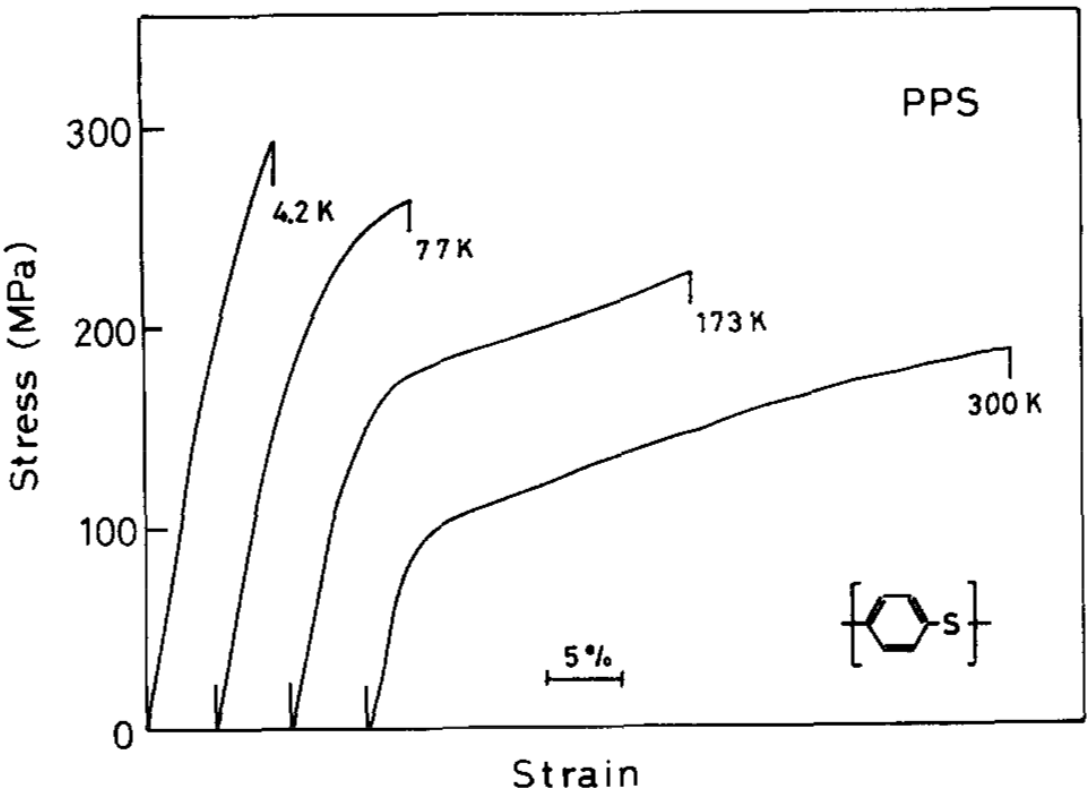

Figure 2.13: Stress-Strain curves for PPS at different temperatures [84]

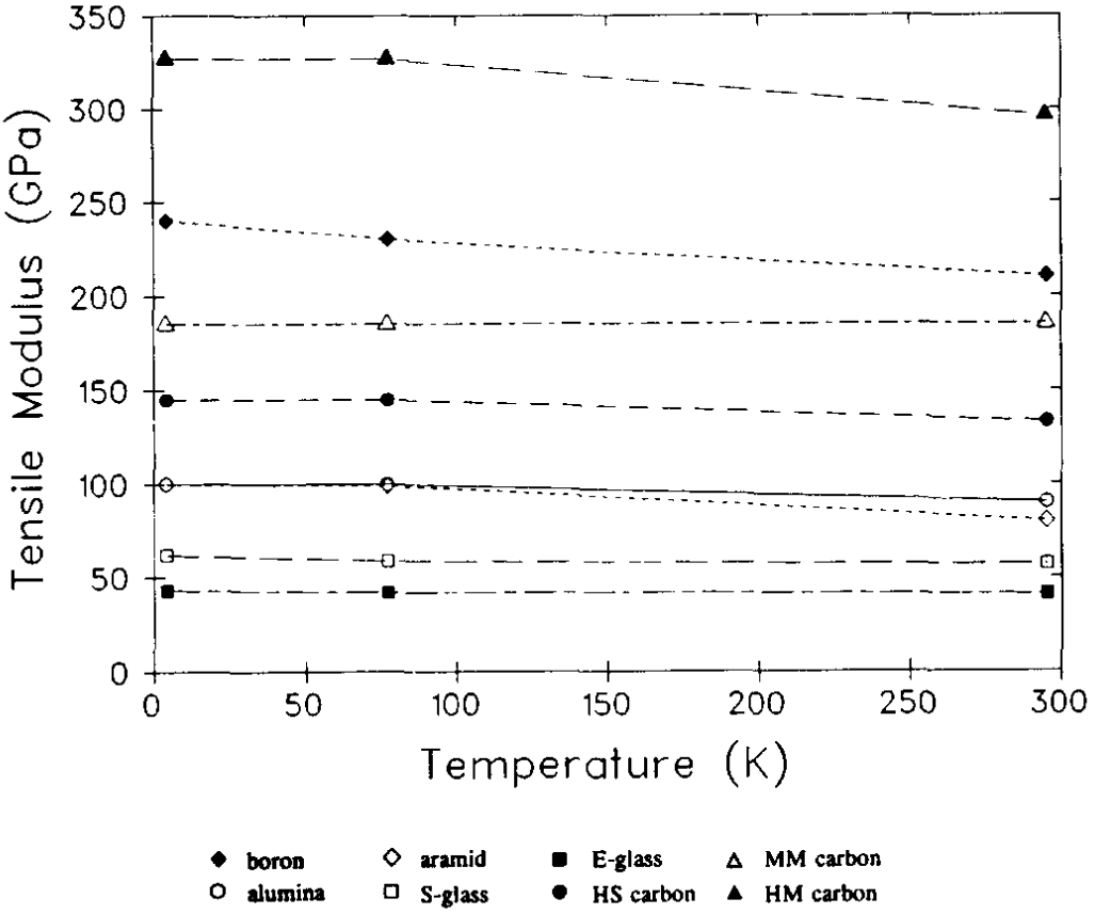

Figure 2.14: Tensile modulus of unidirectional fiber-reinforce laminates [67]

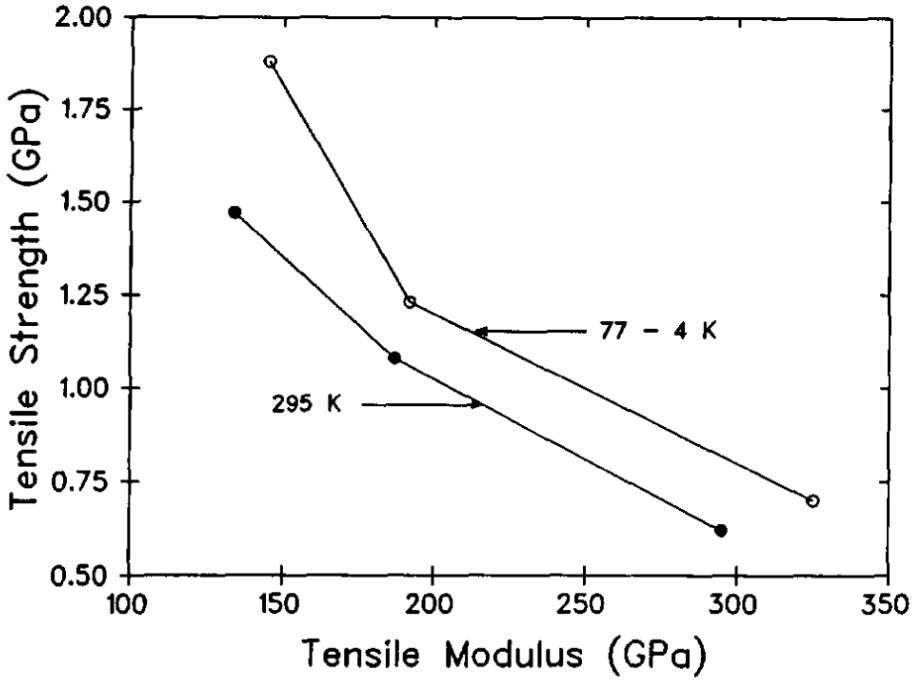

Figure 2.15: Tensile strength versus tensile modulus of carbon fibre for three different grades [67]

Furthermore, the high stress environment caused by exposure to cryogenic temperatures leads to diverse issues. These issues arise due to factors such as matrix shrinkage during curing, Poisson's effects, and differences in thermal expansion coefficients between fibers, matrix, and neighboring ply groups in laminates. In cryogenic liquid storage systems, small-scale damage can escalate with repeated cycling, leading to structural failure due to inadequate consideration of microcracking and thermal stress. Thermal stresses perpendicular to the fibers in laminates can cause failure, ultimately resulting in debonding and transverse crack formation, as can be seen in Figure 2.16 [79].

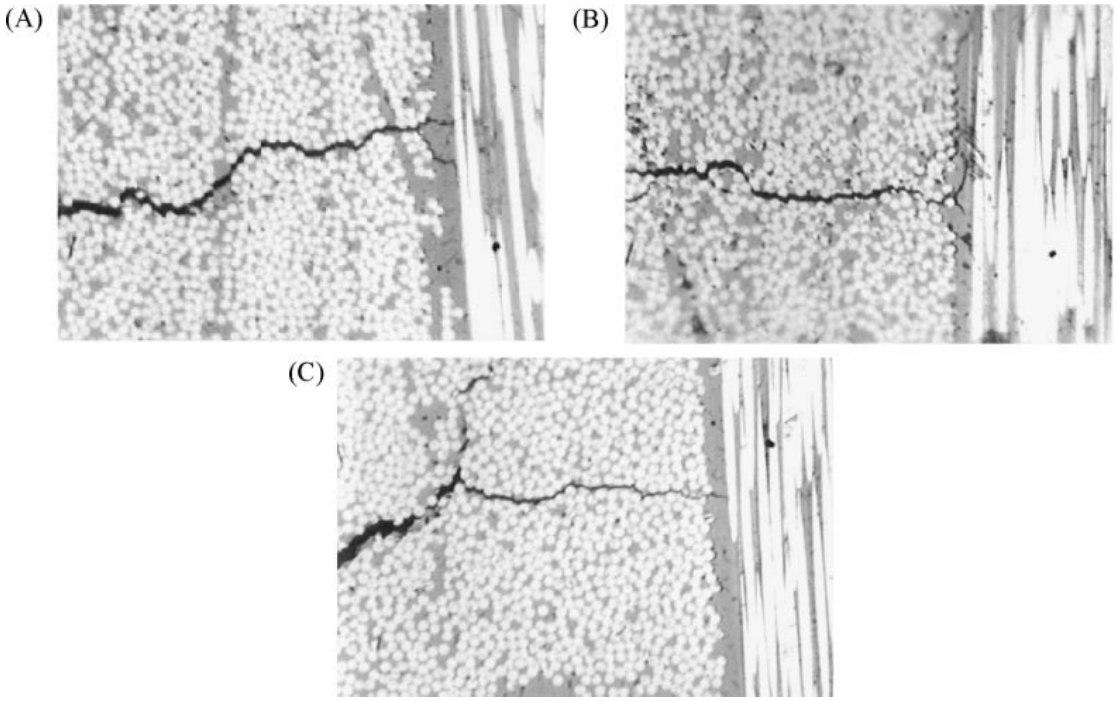

Figure 2.16: Micro cracks in the composite after a cryogenic cycle [79]

2.6 Simulations

The design, optimization, and certification of composite hydrogen vessels represent a significant engineering problem. The extreme operating conditions, complex material behavior, and stringent safety requirements make empirical testing both economically unfeasible and time-consuming. Consequently, high-fidelity computational modeling and Finite Element Analysis (FEA) have become crucial for the development cycle [43].

The simulation of high-pressure composite vessels for storing gaseous hydrogen has matured significantly. The foundational task is ensuring structural integrity under high internal pressure, for which deterministic FEA is the primary tool [43].

A key aspect of this analysis is the prediction of failure. This is achieved by implementing various failure criteria in the FEA as shown in Table 2.3. Physically-based, mode-specific criteria like the Hashin and Puck criteria are largely adopted as these models offer a more nuanced prediction of damage initiation [55, 86].

Model/Criterion	**Type**	**Physical Basis**	**Predicted Failure Modes**	**Source**
Maximum Stress/Strain	Limit Criterion	Non-interactive; compares individual stress/strain components to their respective limits.	Fiber/Matrix Tension/-Compression, Shear	[18]
Tsai-Hill	Interactive Criterion	Based on distortion energy, it extends the von Mises criterion for anisotropic materials.	Combined stress state failure.	[18]
Tsai-Wu	Interactive Criterion	A general quadratic tensor polynomial that includes interaction terms between stress components.	Combined stress state failure.	[43]
Hashin	Mode-Specific	Physically-based, with separate criteria developed for fiber and matrix failure modes.	Fiber Tension/Compression, Matrix Tension/Compression.	[86]
Puck	Mode-Specific	Micromechanics-based, focusing on fracture plane analysis for inter-fiber failure (IFF).	Fiber Failure, Inter-Fiber Failure (IFF) with multiple modes.	[55]
PDM via CDM*	Damage Evolution	Uses internal damage variables to model stiffness degradation post-failure initiation.	Progressive evolution of all modes (Matrix Cracking, Delamination, Fiber Breakage).	[86]

*Progressive Damage Model via Continuum Damage Mechanics

Table 2.3: Overview of Failure Criteria and Damage Models for Composite Vessels

To capture the gradual failure process and load redistribution that occurs after initial damage, Progressive Damage Modeling (PDM) has become the state-of-the-art deterministic approach [86]. PDM uses internal damage variables to model the degradation of material stiffness after failure initiation, providing a more complete picture of the vessel's behavior up to burst.

While deterministic FEA provides a single-value prediction for burst pressure, it cannot account for the inherent variability in material properties, manufacturing processes, and operational loads. This has driven a shift towards probabilistic and reliability-based design methods. The Monte Carlo Simulation is a prominent technique used to assess the impact of these uncertainties, providing a bridge between idealized simulation and experimental reality [4].

Furthermore, the design of high-pressure tanks involves multiphysics challenges beyond simple structural mechanics. The introduction of Type IV vessels brought the complex failure mode of liner collapse. This phenomenon is driven by the permeation of small hydrogen molecules through the polymer liner. During a rapid depressurization event, hydrogen trapped at the liner-composite interface cannot escape quickly enough, creating a pressure differential that can cause the liner to buckle inward [24, 62]. Accurately simulating this requires a coupled diffusion-mechanical analysis.

Another critical challenge is the significant temperature rise during fast refueling. This requires moving beyond pure structural mechanics into the realm of computational fluid dynamics to model the thermodynamic effects of gas compression and ensure the vessel remains within safe thermal limits [31].

While the simulation of high-pressure gas tanks has reached a considerable level of maturity, the analysis of composite vessels for storing liquid hydrogen presents a different set of challenges. The physics of the cryogenic environment fundamentally alters the material behavior, the dominant loading conditions, and the primary failure mechanisms. In fact, for any structure operating at 20 K, thermal and mechanical analyses are inextricably linked. The massive temperature differential from an ambient fabrication temperature (293 K) to the cryogenic operating temperature (20 K) becomes a dominant source of stress. As detailed in Section 2.5, the primary driver of this stress is the mismatch in the CTE between the composite's fibers and matrix [65].

Therefore, a coupled thermo-structural analysis is the absolute foundation for simulating LH2 tanks. The standard workflow involves a two-step FEA process. First, a thermal analysis determines the temperature distribution throughout the structure, and second, this temperature field is imported as a body load into a structural analysis to calculate the resulting stresses and deformations [76].

The phenomena of microcracking adds another layer of complexity to the analyses, as cracks can coalesce and interconnect between adjacent plies, forming continuous leak paths through the tank wall [34, 49].

Predicting this brittle fracture requires sophisticated tools beyond standard failure criteria. The research focus has therefore shifted to a tighter integration of advanced simulation with rigorous experimental validation. On the simulation side, methodologies like Fracture Mechanics and the use of the Energy Release Rate (ERR) as a design objective are employed [30]. To achieve the highest fidelity, trans-scale modeling frameworks are also being developed. These connect the microscopic behavior of fibers and matrix within a Representative Volume Element (RVE) to the macroscopic performance of the entire tank, providing a more physically accurate prediction of performance [40, 53].

The development and validation of these advanced models are, however, critically dependent on experimental data. This essential research involves performing cryogenic thermal cycling on composite coupons and examining the resulting microcrack density with scanninge electron microscopy to validate the damage models [79] and investigating the cryogenic performance of new materials, such as thinner prepreg plies or toughened resins, to provide accurate input data for simulations [54, 77].

This synergy between predictive modeling and physical testing is crucial for advancing the research of cryogenic storage vessels, most notably the development of linerless tanks. In such designs, the composite itself must serve as an impermeable barrier. The microcracks are no longer just a structural concern but become direct pathways for leakage, demanding a deep, validated understanding of permeability through damaged media [7, 34, 49].

In Table 2.4 is possible to find an overview of the different simulation approaches for compressed and liquid hydrogen tanks.

Table 2.4: Comparison of High-Pressure and Cryogenic Hydrogen Vessels simuations

Analysis Aspect	High-Pressure Vessels	Cryogenic Vessels
Primary Storage State	Compressed Gas	Cryogenic Liquid
Operating Temperature	Ambient, with excursions (233 K to 358 K)	Cryogenic 20 K
Primary Mechanical Load	High Internal Pressure (350 bar to 700 bar)	Moderate Internal Pressure (typically <10 bar)
Dominant Thermal Load	Transient heating during fast refueling (~293 K to ~360 K)	Extreme, steady-state cold and thermal shock during cooldown (~293 K to 20 K)
Key Failure Modes	Burst, Liner Buckling/Collapse, Fatigue, High-Temp Material Degradation	Thermally-induced Matrix Microcracking, Delamination, Low-Cycle Thermal Fatigue, Boil-off
Critical Component/Interface	Polymer Liner / Composite Interface	Composite Laminate Interfaces, Structural Supports (Thermal Bridging)
Primary Simulation Challenge	Coupled Diffusion-Mechanical analysis for liner collapse; Coupled CFD-Thermal analysis for refueling.	Coupled Thermo-Structural-Damage analysis for composite integrity; Heat transfer analysis for boil-off.
Permeability Model Focus	Gas diffusion through an intact polymer liner.	Fluid flow through a network of damage-induced microcracks in the composite.

2.7 Research Gap

Composite materials are highly valued for creating strong, lightweight hydrogen tanks. The performance of these composite structures significantly depends on the materials used, a fact well-supported by research. New materials, such as thermoplastics, are of particular interest due to their potential for improved toughness, faster manufacturing, and recyclability. Another crucial design decision is the inclusion and material type of a liner, as this choice profoundly impacts the tank's permeability and overall performance, especially in the context of creating linerless vessels.

While numerous studies have established a mature field around the design and analysis of composite vessels for storing compressed hydrogen [8, 9, 11, 15, 28, 30, 37, 46, 56, 64, 69, 70, 86], far fewer investigations have focused on the unique challenges of composite tanks for liquid hydrogen storage [12, 30, 34, 40, 58, 76, 80].

The fundamental challenge for LH2 storage vessels shifts from managing high internal pressure to mitigating the effects of extreme cryogenic temperatures (20 K). As detailed in the previous sections, this introduces a different physical paradigm. The primary driver of failure is no longer burst pressure but the severe thermally-induced stress from the mismatch in thermal expansion coefficients between the fiber and matrix. This stress leads to the critical failure mode of matrix microcracking, which can create leak paths and compromise the vessel's integrity.

Consequently, a significant research gap exists in the predictive simulation of how different composite material systems, particularly emerging thermoplastics, behave under these specific cryogenic conditions. While simulation for compressed hydrogen tanks is well-developed, robust modeling of the coupled thermo-structural phenomena and resulting microcrack damage in LH2 tanks is an area requiring further research.

Given the cost and complexity of extensive cryogenic testing, high-fidelity simulation is the most effective tool for initial design exploration. The scope of this thesis is therefore to address this gap by developing and employing a coupled thermo-structural Finite Element Model. This model will be used to analyze and compare different tank configurations, specifically focusing on the performance of various thermoplastic matrices. By predicting the thermally-induced stress fields and the onset of matrix damage, this work aims to provide a clear comparison of material performance, making it possible to identify the most promising candidates for future manufacturing and experimental testing. In the following sections, the methodology for this analysis will be introduced and the results will be discussed.

Chapter 3

Methodology

3.1 Geometry and Model Setup

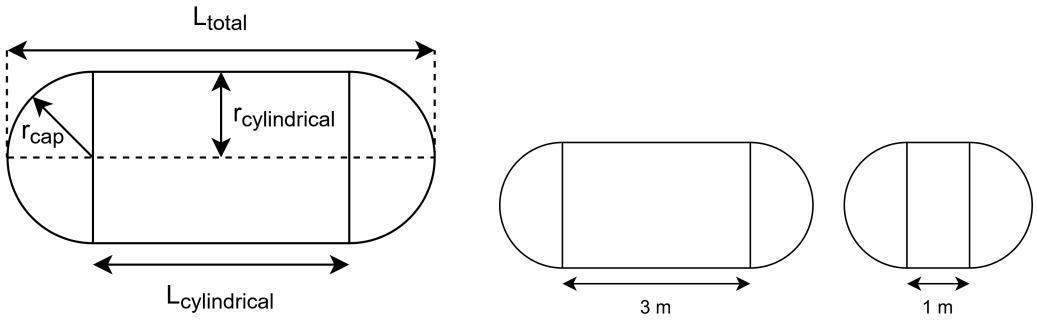

(a) Tank geometry and key parameters. **(b)** The two geometric variations analyzed.

Figure 3.1: Overview of the tank geometries studied.

The analyses in this study were conducted using ANSYS Workbench, a well established FEA simulation tool with high capabilities in composite materials simulation.

The model considers a cylindrical tank with hemispherical end caps, as illustrated in Figure 3.1a. To analyze the effect of scaling on performance, two variations of the geometry were modeled, differing only in the length of their cylindrical sections. The key dimensions for both tank configurations are summarized in Table 3.1.

Table 3.1: Key dimensions for the two tank configurations.

Parameter	Symbol	Tank 1	Tank 2
Cylindrical Shell Radius	$r_{cylindrical}$	1 m	1 m
Cylindrical Shell Length	$L_{cylindrical}$	3 m	1 m
Spherical Cap Radius	r_{cap}	1 m	1 m
Total Length	L_{total}	4 m	2 m

Recognizing the symmetrical nature of the problem, the model was simplified to represent only an eighth of the full tank geometry, as shown in Figure 3.2.

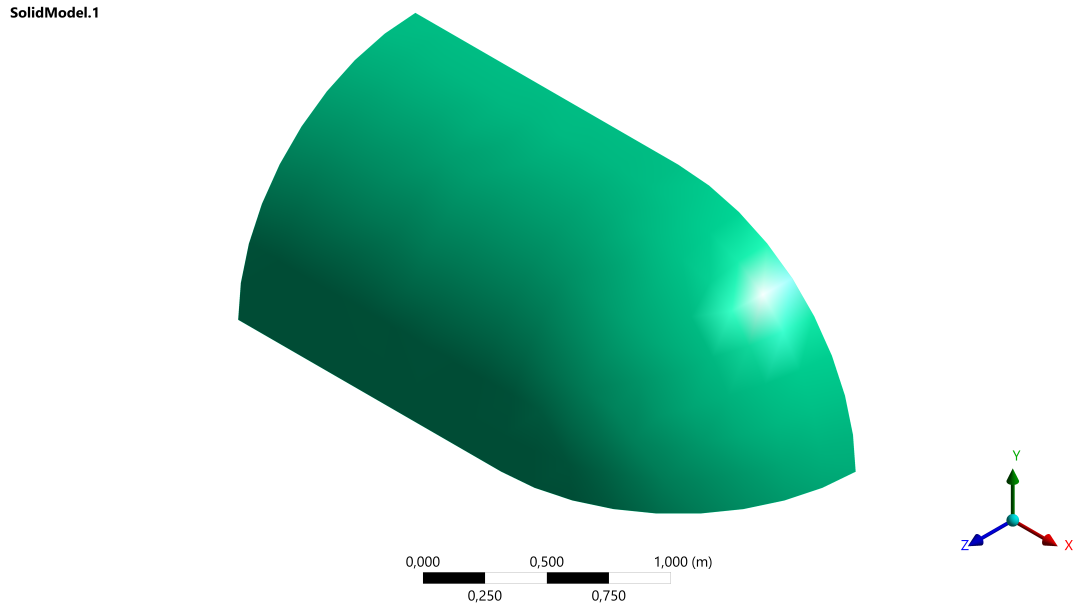

Figure 3.2: Tank Model

This simplification significantly decreased the computational resources and time needed for the analysis.

3.1.1 Composite layup and liner definition

ANSYS ACP (Pre/Post) was utilized for the specific task of defining the composite model. The laminate was constructed based on a repeating fundamental group of plies. This fundamental building block is an 8-ply, balanced laminate defined by the sequence $[0/45/90/45]_2$. Considering a nominal per-ply thickness of 0.1mm, this 8-ply stack has a cumulative thickness of 0.8mm. The final composite laminate is then fabricated by sequentially stacking this fundamental 8-ply group until the target component thickness is reached. Finally, the newly created composite model is exported to the analyses as solid elements model.

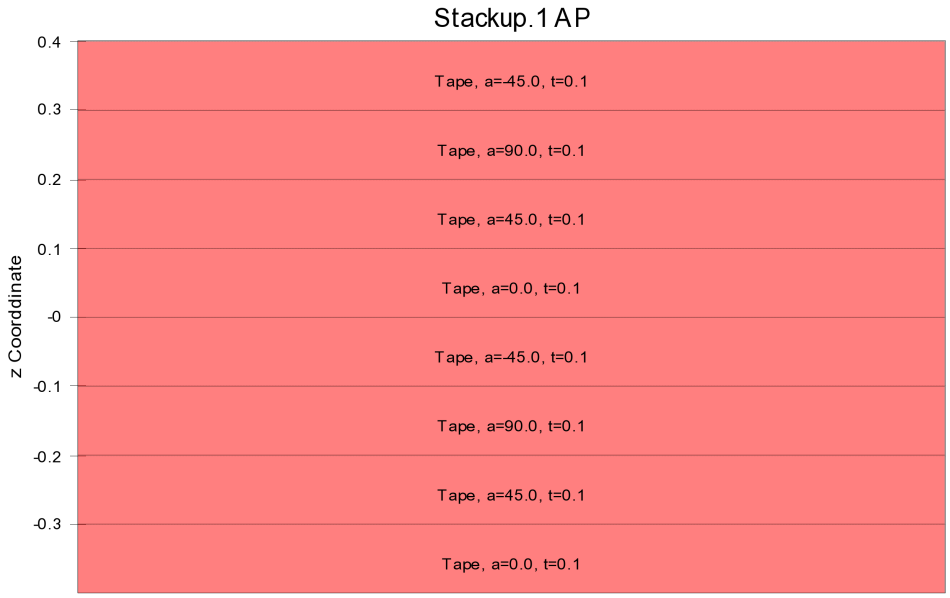

Figure 3.3: Layup sequence

For simplicity, the liner was defined within ACP as a distinct layup sequence consisting in a single isotropic ply of the desired thickness.

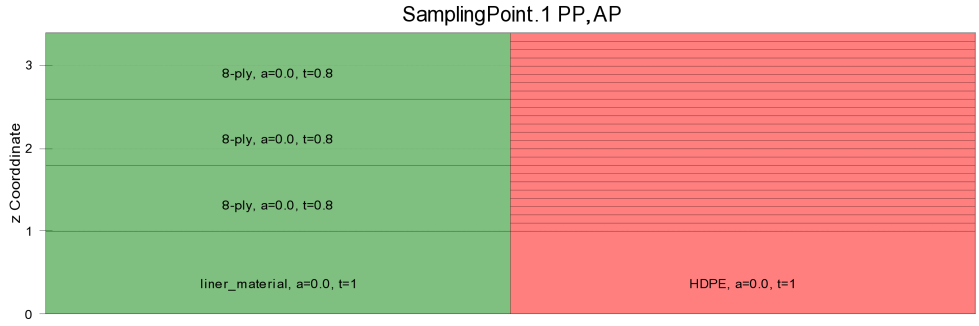

Figure 3.4: Example of the laminate structure with a liner, the 8-ply block has been repeated 3 times to achieve a desired thickness of 2.4 mm

3.2 Materials Creation

With the geometric and composite models established, the subsequent phase of the analysis involves defining the material properties. This study considers several composites formed using two reinforcing fibers, Carbon and Glass, and four thermoplastic matrices: Polyphenylene Sulfide (PPS), Polyetheretherketone (PEEK), Polyamide 6 (PA6), and Low-Melt Polyaryletherketone (LM-PAEK).

A key objective of this study is to investigate the liner's role, therefore two distinct liner materials were chosen. A conventional High-Density Polyethylene (HDPE) liner was selected, alongside an Extended Matrix Liner. The latter concept involves using the composite's matrix material as the liner, allowing for an assessment of the benefits of a material-matched interface. A complete summary of all materials is provided in Table 3.2.

Fiber	**Matrix**	**Liner**
Carbon	PPS	HDPE
Glass	PEEK	Extended Matrix Liner
	PA6	
	LM-PAEK	

Table 3.2: Available materials for the simulation

The composite materials used in this research were generated within ANSYS using the Material Designer module, which allows for the modeling of both mechanical and thermal properties of the matrix and fibers. The first step in the analysis involved the creation of the material model, followed by its validation to ensure accuracy.

Validation of the material model was performed by conducting a thorough review of relevant studies [12, 17, 33, 80, 83], which identified the work by Grogan [33] as the most suitable reference. The reference material was Suprem T/60/IM7/PEEK/150, a composite tape containing a 60% fiber volume of IM7 carbon fibers in a PEEK matrix. Ansys was used to simulate various CF/PEEK composites, with IM7 and other types of carbon fibers, with Grogan's material serving as the baseline for comparison. To ensure a consistent analysis, all simulated materials were assigned a 60% fiber volume fraction and a 7 μm fiber diameter. The initial validation was conducted at room temperature, with the comparative results shown in Table 3.3. Noticeable discrepancies between simulated and literature data are likely attributable to variations in manufacturing processes and raw material characteristics, which are known to significantly influence final composite properties.

Property	**Grogan**	**PEEK/IM7**	**PEEK/CF**	**PEEK/T700S**	**APC-2/IM7**
Room Temperature (23°C)					
Density [kg m^{-3}]	1598	1592	1604	1604	1598
E_1 [GPa]	134	167	176	139	172
E_2 [GPa]	10.3	16.9	10.8	16.7	10
G_{12} [GPa]	6	6.40	4.04	6.33	5.50
ν_{12}	0.32	0.30	0.245	0.30	0.27
k_1 [Wm^{-1}K^{-1}]	3.5	4.2	1.31	5.74	—
k_2 [Wm^{-1}K^{-1}]	0.4	1	0.4	1.06	—
α_1 [$\times 10^{-6}$ K^{-1}]	0.2	-0.12	0.51	0.225	—
α_2 [$\times 10^{-6}$ K^{-1}]	28	19.4	20.8	19.5	—
Cryogenic Temperature (-196°C)					
Density [kg m^{-3}]	1598	1592	1604	1604	—
E_1 [GPa]	152	168	176	140	—
E_2 [GPa]	9.50	22.6	13	13	—
G_{12} [GPa]	4.40	8.55	4.84	8.42	—
ν_{12}	0.32	0.30	0.24	0.30	—
k_1 [Wm^{-1}K^{-1}]	3.5	4.16	1.27	5.69	—
k_2 [Wm^{-1}K^{-1}]	0.4	0.63	0.35	0.62	—
α_1 [$\times 10^{-6}$ K^{-1}]	0	-0.45	0.167	-0.178	—
α_2 [$\times 10^{-6}$ K^{-1}]	24.7	4.38	5.09	4.52	—

Table 3.3: Comparison of different CF/PEEK composites properties at room and cryogenic temperatures

Despite these variations, the elastic moduli in the fiber direction were found to be of comparable magnitude across the different materials. Additionally, the density, shear moduli, and Poisson's ratios were in close agreement, indicating consistency across the materials. The thermal expansion coefficients and thermal conductivity values also showed good correlation with values reported in the literature.

To further validate the thermal conductivity results, a comparison was made with analytical predictions using:

$$k_1 = V_m k_m + V_f k_f \quad \text{and} \quad k_2 = k_m + \frac{V_f}{\frac{1}{k_f - k_m} + \frac{V_m}{2k_m}} \tag{3.1}$$

where k_1 is the thermal conductivity in the fiber direction, k_2 is the thermal conductivity in the transverse direction, k_m and k_f are respectively the thermal conductivity of the matrix and the fiber, V_m is the matrix volume content and V_f is the fiber volume content.

The simulation results were found to be in good agreement with the analytical results, confirming the accuracy of the simulations.

At cryogenic temperatures, the composite materials demonstrated behavior consistent with the expected trends for such materials, reinforcing the validity of the material model under these conditions. Therefore, the model can be considered valid for further use in the creation of the other composites. Moreover, to maintain consistency with the reference study [33], all CF composites were modeled using IM7 carbon fibers. This approach made it possible to isolate the properties of the polymer and better assess its contribution to the overall performance later in the study.

As the availability of comprehensive data at cryogenic temperature for all the materials involved in the analysis is scarce, there's the need of an interpolation, therefore property data for all materials where interpolation was needed, as indicated in the following tables, was calculated according to Table 3.4.

Property	**Change (%)**	**Source**
Density	Negligible	[71]
CTE (in the range 20–77 K)	-40	[26, 39, 44, 73]
Tensile Modulus (Fiber, E_1)	+15	[39, 42, 67, 71, 73]
Tensile Modulus (Transverse, E_2)	+30	[39, 42, 67, 71, 73]
Shear Modulus (G_{12})	+30	[39, 42, 67, 71, 73]
Tensile Strength	+40	[39, 42, 67, 71, 73]
Compressive Strength	+40	[39, 67, 73]
Shear Strength	-15	[42, 67, 71]
Thermal Conductivity	Analytically Computed	

Table 3.4: Approximate Changes in Composite Properties at Cryogenic Temperature (primarily 77 K)

Given the difficulty to retrieve comprehensive data at LH2 temperature (20 K), the values at 77 K were used for the analyses.

	Polymer				**Fiber**	
Property	LM-PAEK	PPS	PEEK	PA6	CF	GF
Density	RC	RC	RC	RC	RC	RC
CTE	R	R	RC	R	RC	RC
Tensile Modulus	R	R	RC	R	RC	RC
Shear Modulus	R	R	RC	R	RC	RC
Thermal Conductivity	R	R	RC	R	RC	RC

R Room Temperature (295 K) RC Both Room and Cryogenic Temperatures (20K-77K)

Table 3.5: Polymer and Fiber Data Availability

The properties of the constituents have been used as is for the creation of the desired composite materials. The materials for which constituents data was available only for Room Temperature have been varied following the parameters in Table 3.4.

The following table shows which property for each material subject to the analysis has been fully or partially interpolated, and which was possible to be found in literature.

	Material				
Property	CF/LM-PAEK	CF/PPS	CF/PEEK	CF/PA6	GF/PEEK
Density	●	●	●	●	●
CTE	●	○	●	○	●
Tensile Moduli	○	○	●	○	◐
Shear Moduli	○	○	●	○	◐
Tensile Strength	○	○	○	○	○
Compressive Strength	○	○	○	○	○
Shear Strength	○	○	○	○	○
Thermal Conductivity	◐	◐	●	◐	●

●: Full Data Set ◐: Partially Interpolated ○: Fully Interpolated

Table 3.6: Data Quality at Cryogenic Temperatures

3.3 Loads, Constraints, and Analysis Parameters

A couple static thermal-structural analysis was set up to evaluate the behaviour of the composite tank. The first step would be to define the thermal loads. On the inner wall of the tank has been applied a temperature of 20 K, corresponding to the temperature of liquid hydrogen. Then, as cryogenic tanks are usually encased in a multi layer insulation system under vacuum to minimize the heat transfer between inner and outer wall, it would be necessary to model the insulation layer itself. However, to reduce the cost and complexity of the simulations, the MLI/Vacuum system has been simplified into a single radiation boundary condition applied to the outer wall. The radiation load has been set with an emissivity of 0.04, typical value for MLI systems [20, 41].

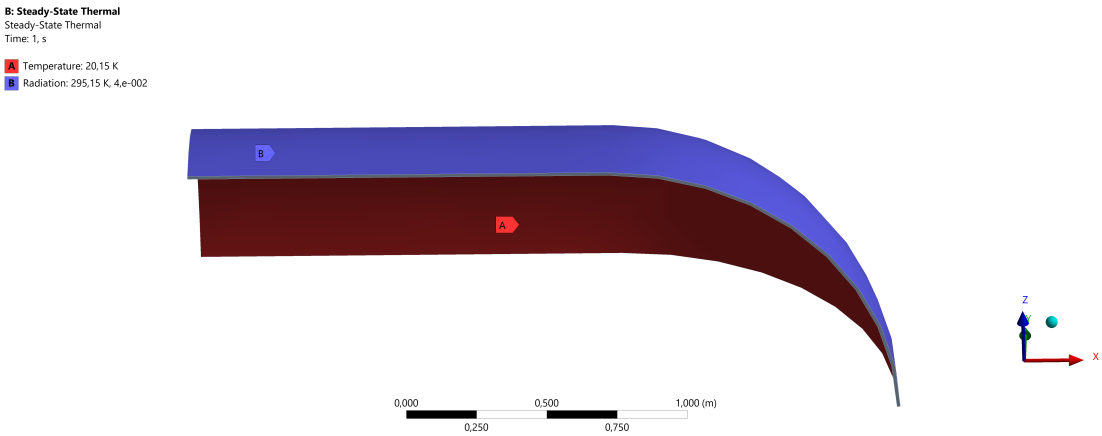

Figure 3.5: Thermal loads applied to the structure

Successively the loads and constraints for the structural analysis have been defined. A pressure load has been applied on the inner wall of the tank to simulate the operative pressure. On each cutout, the displacement in the direction normal to the corresponding plane has been constrained, to guarantee congruence conditions in the material.

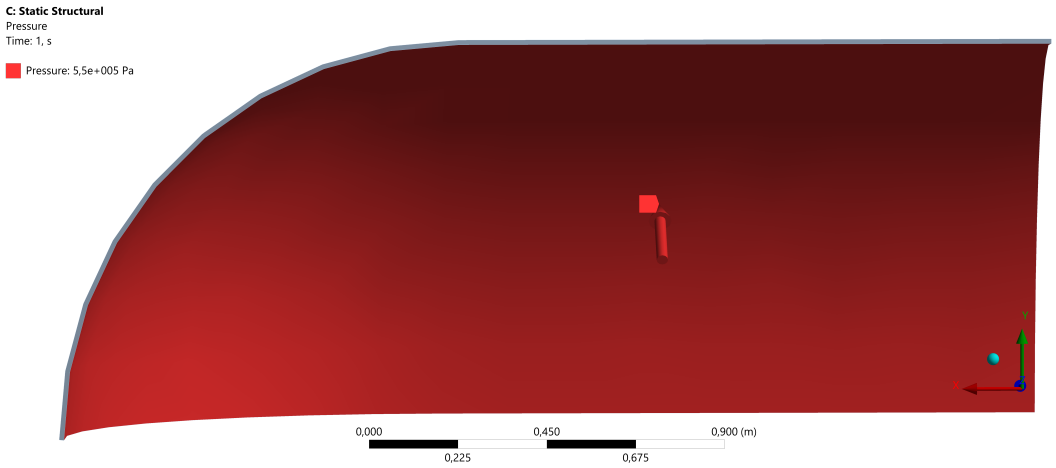

Figure 3.6: Pressure load applied to the structure

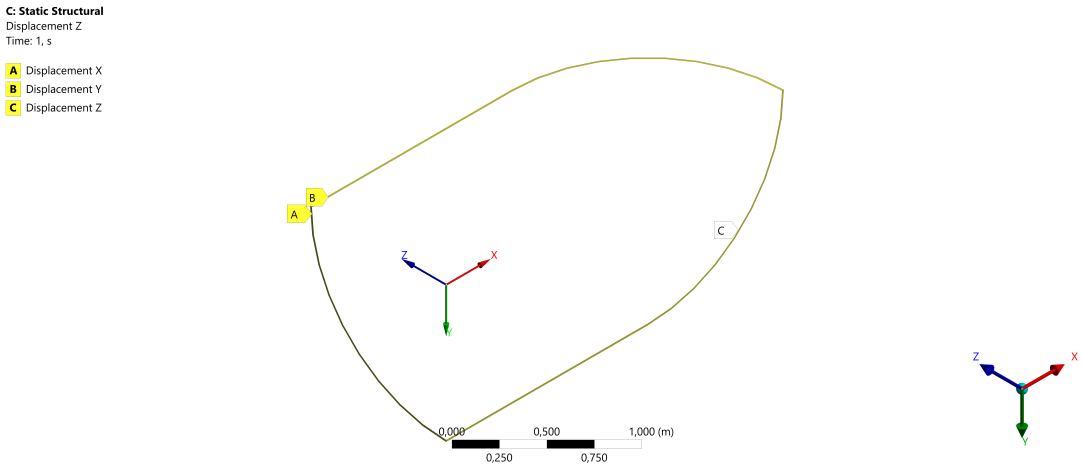

Figure 3.7: Constraints on the three cutout, out-of-plane displacement fixed

The analysis evaluates both strain and stress distributions within the composite structure. To assess the performance of the chosen material, a failure analysis has been conducted. The Inverse Reserve Factor (IRF) was chosen as mean of assessment as it provides a quick way to visualise wether a design is within its limits. An IRF value less than 1.0 signifies that the applied stress is below the material's failure limit. An IRF value equal to or greater than 1.0 suggests that the material has reached or exceeded its limit, and failure is predicted. For instance, an IRF of 1.2 implies the load is 20 percent greater than the stress limit.

Two failure criteria were implemented. For the composite, the Puck criterion was used, as it enables to visualise a more comprehensive failure behaviour, differentiating between various failure modes within fibers and matrix, as exemplified in Figure 3.8.

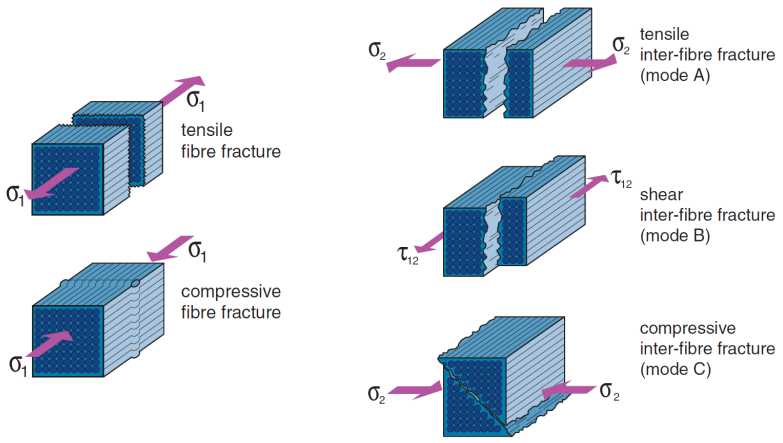

Figure 3.8: Failure modes according to Puck's criterion [5]

For the liner, as it is made from an isotropic material, the Von Mises criterion was used, which compares the Von Mises equivalent stress σ_v to the yield stress of the material, as follows:

$$\sigma_v = \sqrt{\frac{(\sigma_{11} - \sigma_{22}^2 + (\sigma_{22} - \sigma_{33})^2) + (\sigma_{33} - \sigma_{11})^2 + 6(\sigma_{12}^2 + \sigma_{13}^2 + \sigma_{23}^2)}{2}} < \sigma_{yield} \tag{3.2}$$

The two failure criteria are then combined and the IRF is calculated within ANSYS. For the results, the maximum IRF in the structure is taken.

For a tank, Mass and Gravimetric Capacity constitute two important values that need to be considered when assessing its performance, together with the failure behaviour above described. The mass of the tank was valuated by extracting the mass value of the model via ACP, and then multiplied it by 8, to get the full mass. The Gravimetric Capacity was calculated as

$$GC = \frac{M_{LH2}}{M_{LH2} + M_{tank}}$$

where the mass of liquid hydrogen, for simplicity, was considered for an entirely filled tank, as

$$M_{LH2} = \rho_{LH2} \cdot V_{tank}$$

The volume of the tank was calculated by summing the volumes of the cylindrical shell and the two emispherical caps, taking into account the thickness given by the composite and liner, as

$$V_{cylindrical} = \pi(r_{cylindrical} - t_{composite} - t_{liner})^2 \cdot L_{cylindrical}$$

$$V_{sphere} = \frac{4}{3}\pi(r_{sphere} - t_{composite} - t_{liner})^3$$

As IRF, Tank Mass and Gravimetric Capacity are all crucial values to take into account for evaluating the performances of the tank, they have been assembled together into a Performance Index, defined as the geometric mean of their values:

$$F = (\hat{\text{IRF}})^{w_{irf}} \cdot (\hat{\text{GC}})^{w_{gc}} \cdot (\hat{M}_{tank})^{w_m}$$

where w_{irf}, w_{gc} and w_m are the mean weigths respectively for IRF, gravimetric capacity and tank mass. As the contribute of all the variable is considered equally important, the weights are all set equal to 1/3. The IRF, GC and M_{tank} involved in the Perfomance Index calculation were beforehand normalized based on the desired dataset, following:

$$\hat{IRF} = \frac{IRF_{\text{max}} - IRF_{\text{value}}}{IRF_{\text{max}} - IRF_{\text{min}}}$$

$$\hat{GC} = \frac{GC_{\text{value}} - GC_{\text{min}}}{GC_{\text{max}} - GC_{\text{min}}}$$

$$\hat{M}_{\text{tank}} = \frac{M_{\text{tank, max}} - M_{\text{tank, value}}}{M_{\text{tank, max}} - M_{\text{tank, min}}}$$

Where IRF and M_{tank} are equal to 1 for the smallest value of the dataset, and GC is equal to 1 for the highest.

Finally, all the variables under consideration in the analysis have been set in a parametric study, enabling to evaluate multiple combinations and get an overview of how the performance of the composite tank varies with changes in the parameters. All the parameteres utilized in the study have been reported in Table 3.7.

Parameter	**Values**	**Unit**
Shell material	CF/PEEK CF/PPS CF/PA6 CF/LM-PAEK GF/PEEK	—
Shell thickness	2.4, 3.2, 4.8, 7.2, 9.6, 12, 24	mm
Liner material	HDPE Extended Matrix Liner	—
Liner thickness	0, 2.5, 5	mm
Pressure	0.1, 0.325, 0.55, 1.0	MPa
Inner wall temperature	20	K
Emissivity	0.04	—
Cylindrical shell and caps initial radii	1	m
Cylindrical shell length	1, 3	m

Table 3.7: Parameters utilized in the simulations

Chapter 4

Results

4.1 Failure Analysis and Assessment of Liner and Materials influence

The first set of results shows the mechanical behavior of a 12 mm thick CF-PEEK Tank under a 0.55 MPa load.
Deformation (Figure 4.1) is coherent with the expected behavior of thin walled cylindrical vessels, showing a higher magnitude on the longitudinal section compared to the cap section.
Equivalent Von Mises Stress (Figure 4.2) is chosen to display qualitatively how stress is distributed along the structure and follow the same trend and it is possible to see how the longitudinal section presents higher IRF (Figure 4.3) values than the spherical cap, this is due to the fact that cylindrical sections are subject to higher stresses than spherical ones[1]

[1] $$\sigma_{cylinder} = \frac{Pr}{t} > \sigma_{sphere} = \frac{Pr}{2t}$$

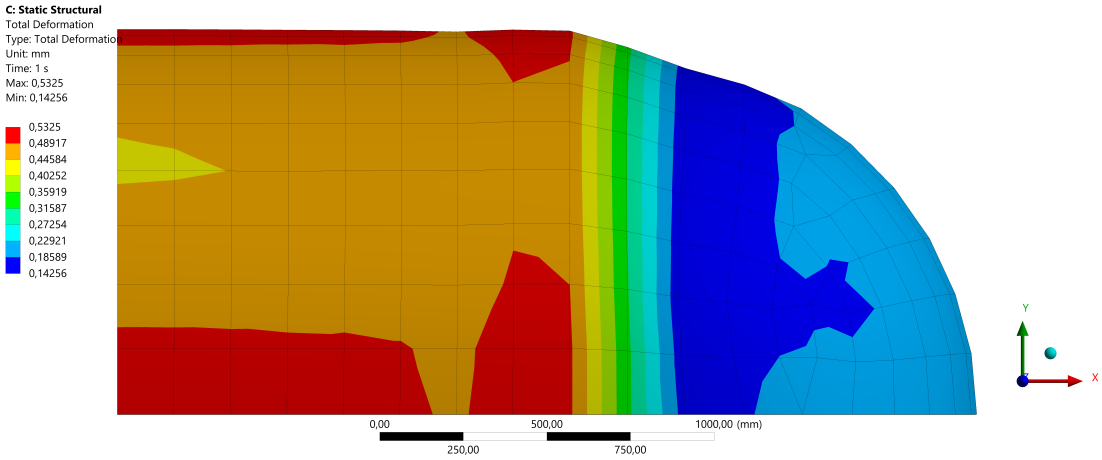

Figure 4.1: Deformation

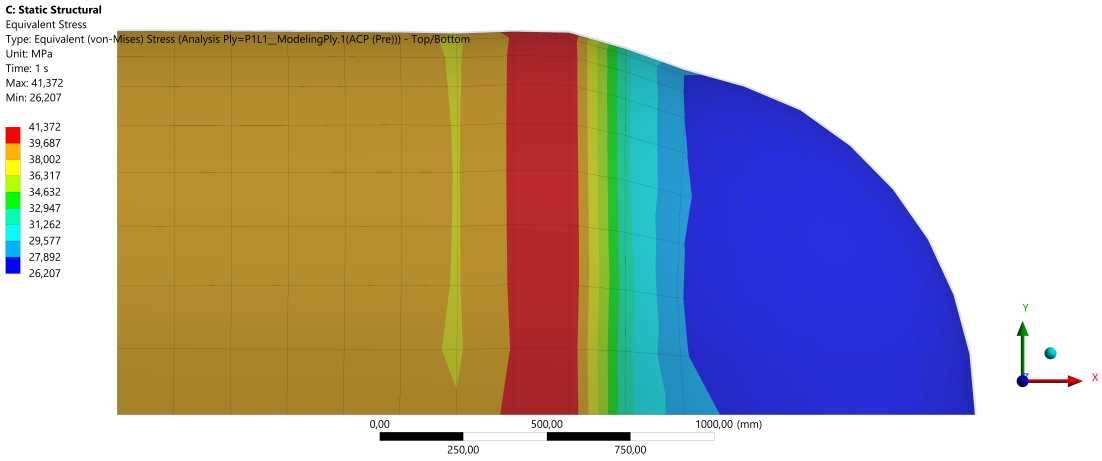

Figure 4.2: Stress Distribution

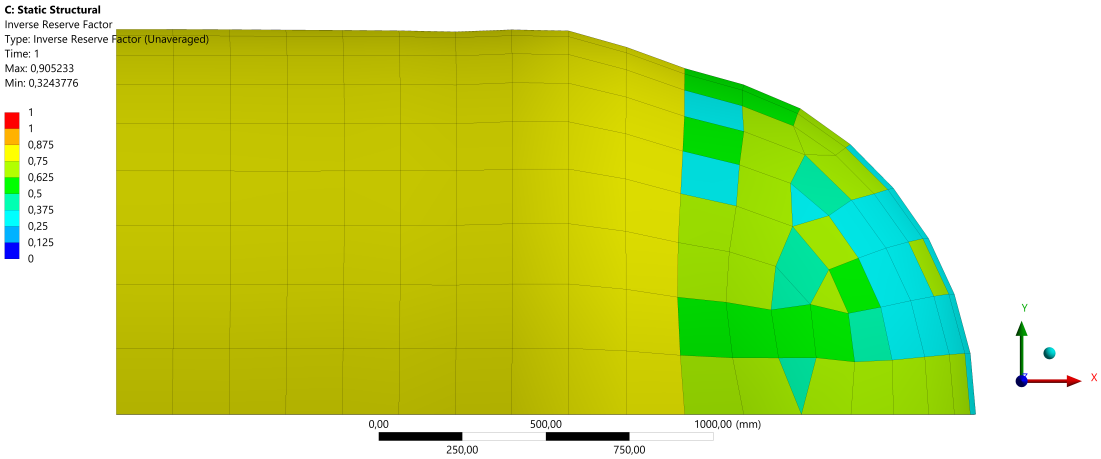

Figure 4.3: Failure Index

Figure 4.4 shows the variation of the IRF correlated to change in wall thickness and pressure. Intuitively, thicker tanks exhibit a higher structural strength than thinner ones.

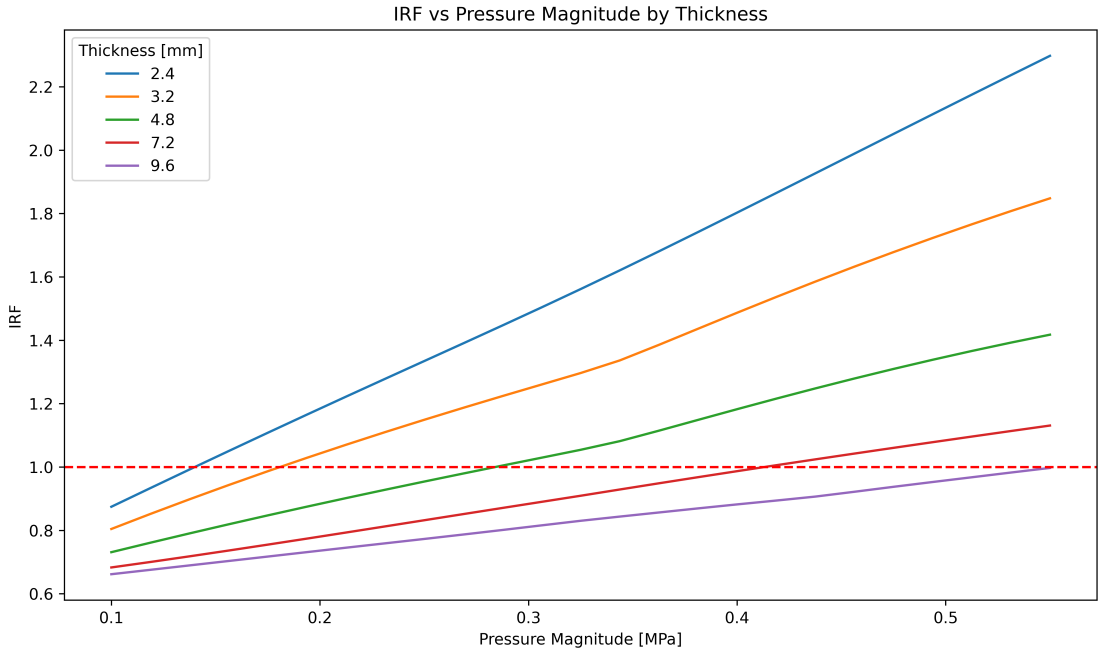

Figure 4.4: Linerless CF-PEEK Tank IRF variation

Once the effect of thickness and pressure has been determined, the successive analyses focused on the impact of different composite materials. After the materials evaluation, an HDPE liner influence has been investigated. For the reader's sake the results for both analyses are summarized in Figure 4.5, showing failure behavior at three significant values of pressure. It is important to state that 1 MPa is

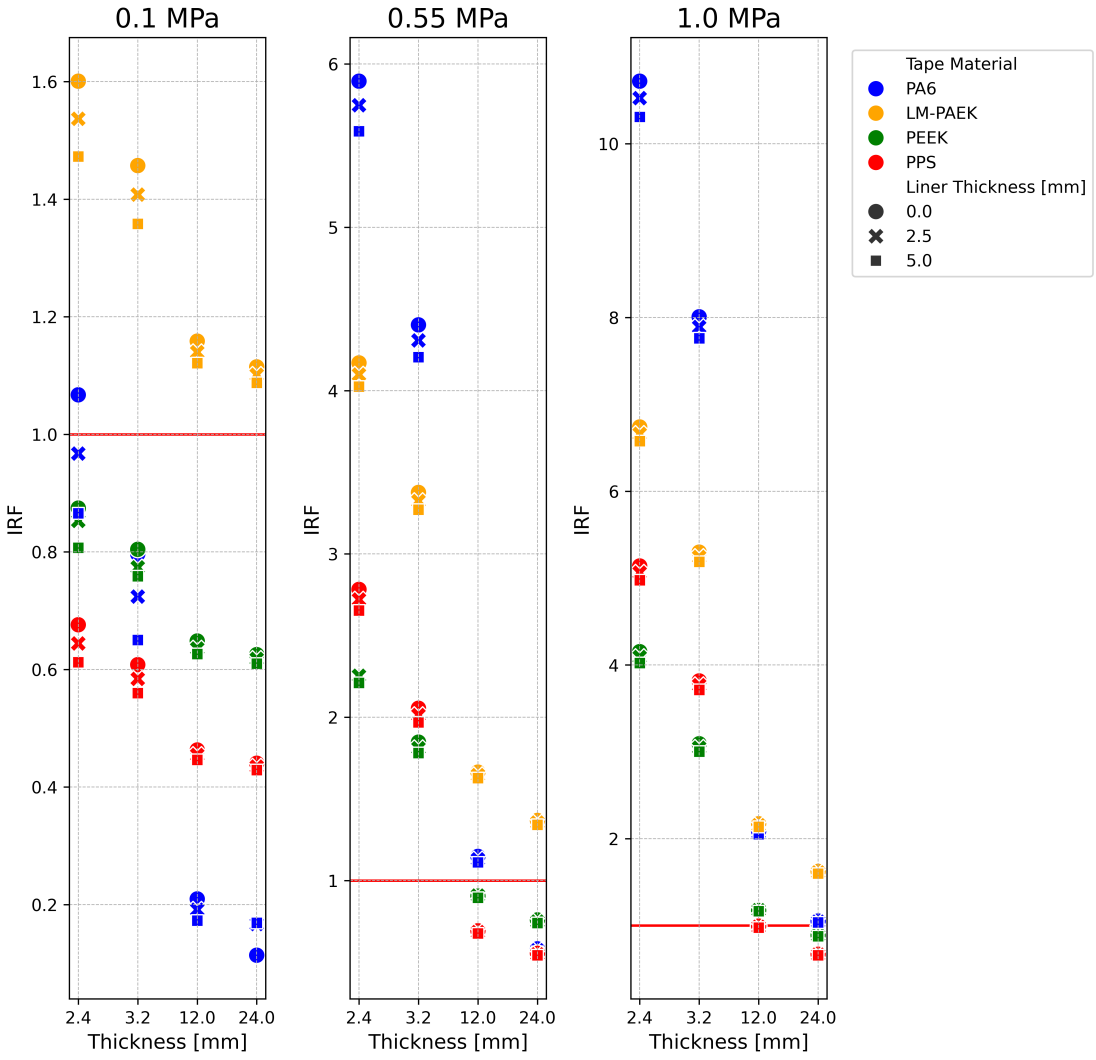

Figure 4.5: Analysis of Failure for different Materials and presence of an HDPE Liner

significantly higher than the functioning pressure of the tank which is 0.2 MPa. To take into account all the loss in accuracy given by the simplifications done in this study a safety factor of 2.75 has been considered, hence 0.55 MPa has been chosen as the design pressure and on which to base comparisons on. Furthermore

as all the studied composite materials are a composition of Carbon Fiber and a polymer, only the name of the latter is shown for convenience in the following results.

Looking at the results, 12 mm is the minimum thickness for which there isn't failure for at least one material. Moreover, PPS and PEEK show to be the best candidates for such thickness. LM-PAEK and PA6 show to be the worst in all cases, with their performance improving for thicker tanks and PA6 surpassing LM-PAEK performances as thickness gets higher.
Concerning the liner presence, it doesn't increase the failure performance on thick tanks, where the liner thickness is overshadowed by the composite's. A different matter occurs for thin composite shells, for which the liner has a significant effect in reducing the IRF.

An interesting observation can be made for the 0.55 MPa and 0.1 MPa cases where, by modifying the pressure or the thickness, the polymer performance ranking changes, leading to cases where PA6 outperforms the other materials. This behavior is likely due to the approximative data, especially strength values, that have been used in the analysis, as they are highly dependant on a wide number of factors like fiber selection, matrix, manufacturing methods etc.

Moreover, as the IRF calculation is based on Puck's criterion and takes account of various fiber and matrix failure modes, the majority of the material presented matrix cracking as critical failure mode, hence a higher or lower IRF indicates the capacity of said material to withstand that fracture mode. As the Puck criterion calculates separate failure indices for distinct modes and the final IRF is determined by the single highest failure index, it is possible that the change in pressure and thickness induces a shift in the critical failure mechanism, which leads to a change in the IRF, which can be higher or lower based on the capacity of the material to withstand the predominant failure mode.

Once the design pressure has been defined, a refinement study has been conducted in an attempt to minimise the thickness. To do so, the analysis objective is to find which thicknessess below 12 mm result in an IRF lower than but close to one and for which materials. Based on their performance in the previous analysis, 2.4 and 3.2 mm have been discarded, and three values of thickness between 12 mm and 3.2 mm have been chosen as refinement values. The results can bee seen in Figure 4.6.

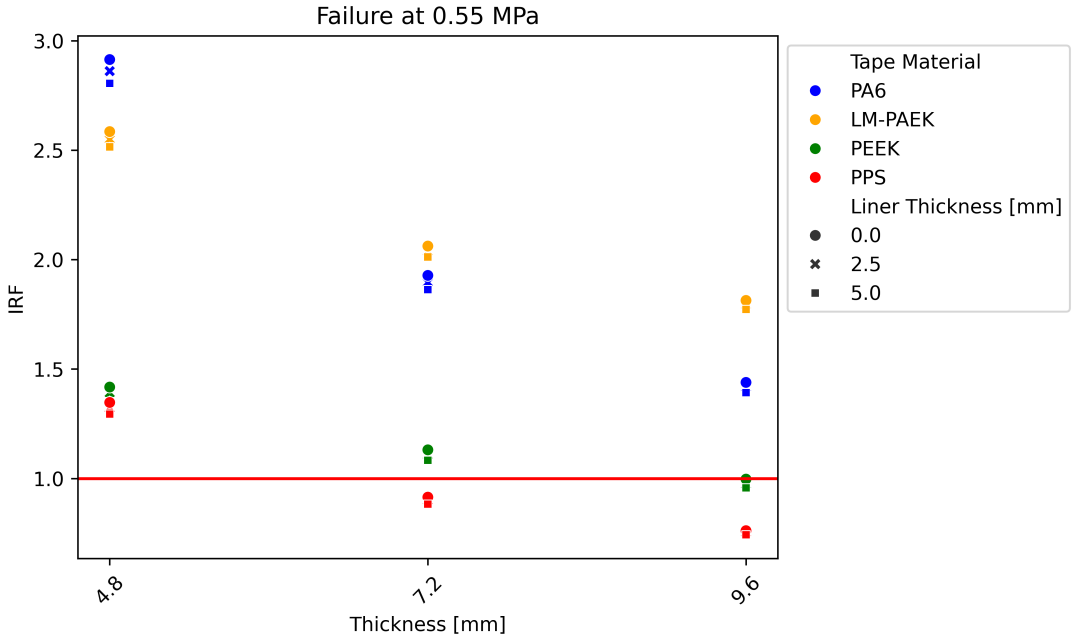

Figure 4.6: IRF for Refined Thickness

From the three values of composite thickness taken into exam, 7.2 mm is the minimum value for which failure doesn't occur in at least one specimen. Here, PPS confirms its position as the best performer. The same happens for 9.6 mm, where PPS is followed by PEEK, but only if the liner is present. Given the choice of a conservative safety factor, it is possible to assume that PEEK and PA6 may be a viable choice, even for the refined thicknessess. Thus, PPS, PEEK and PA6 will be maintained for further analyses. LM-PAEK will be instead discarded as it doesn't yield satisfying results. Both 7.2 mm and 9.6 mm will used from now on as parameters for successive analyses.

4.1.1 Extended Matrix Liner

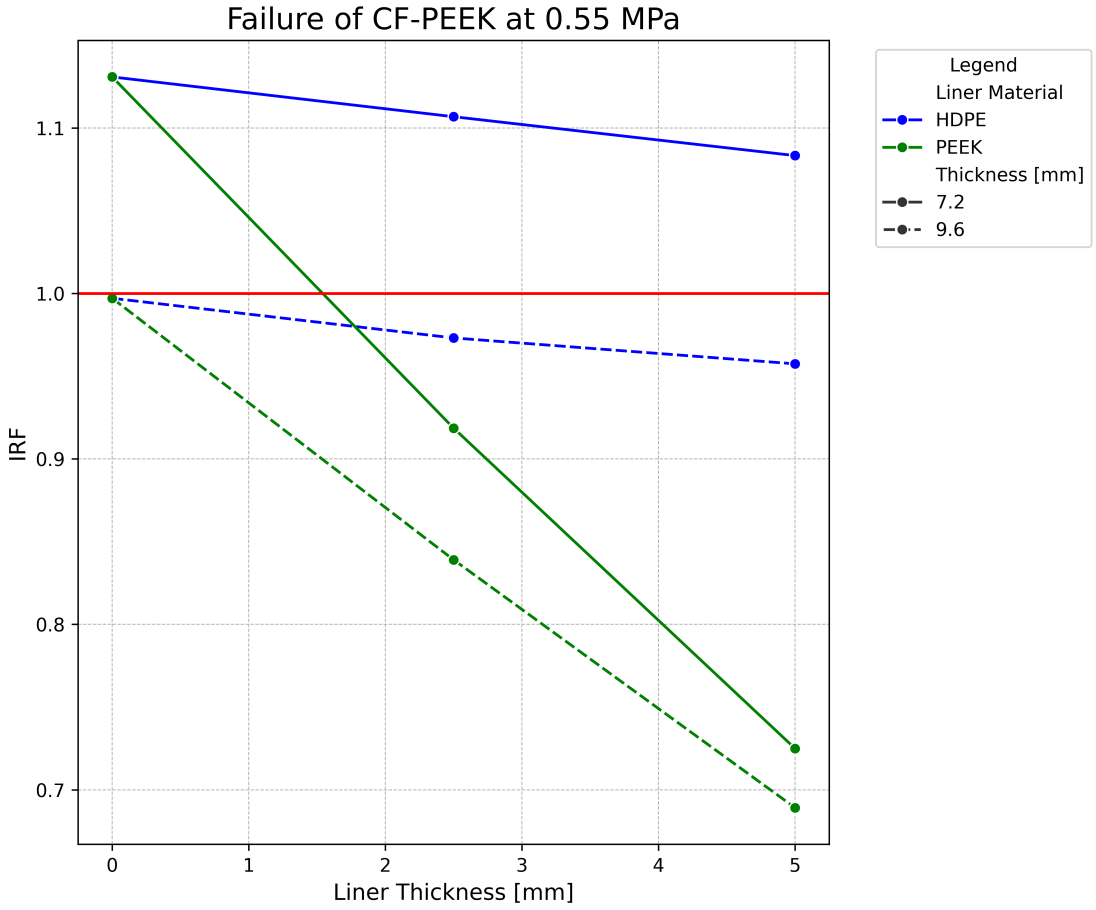

Figure 4.7: Comparison of failure between a PEEK and a HDPE Liner for a CF-PEEK Tank

While the liner influence on failure has been shown for a HDPE liner, it is quite interesting to see if varying the liner material and in particular choosing an extended matrix liner, improves or not the performance of the tank. First of all, a comparison between HDPE and extended matrix is due, and it is shown in Figure 4.7.

As PEEK tensile strength is approximately 4 times higher than HDPE, its use as liner material proves to be a good choice, improving the compatibility between liner and composite layer. PPS and PA6 have been analysed with an extended matrix liner as well, and the results are presented in Figure 4.8.

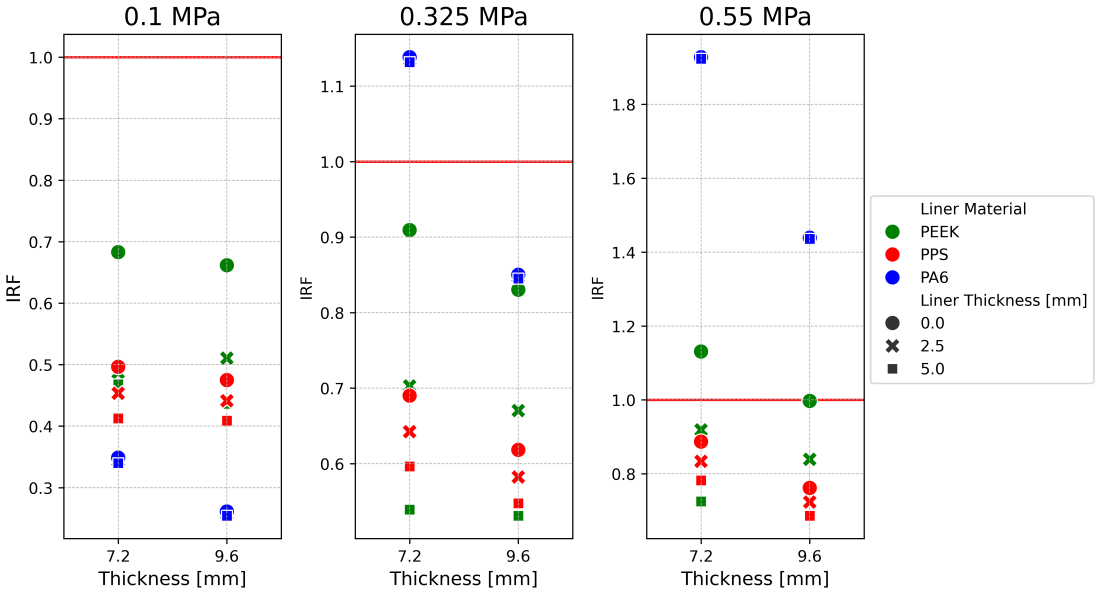

Figure 4.8: Failure of Tanks with an Extended Matrix Liner

All the materials benefit from the extended matrix liner, especially PEEK, which converges on the same performance of PPS or even surpasses them.

4.2 Fiber variation

Given the thermal sensitivity of the composite material properties, another interesting results is given by the comparison between two different fibres with the same polymer. A tank with GF-PEEK has been evaluated and the results shown.

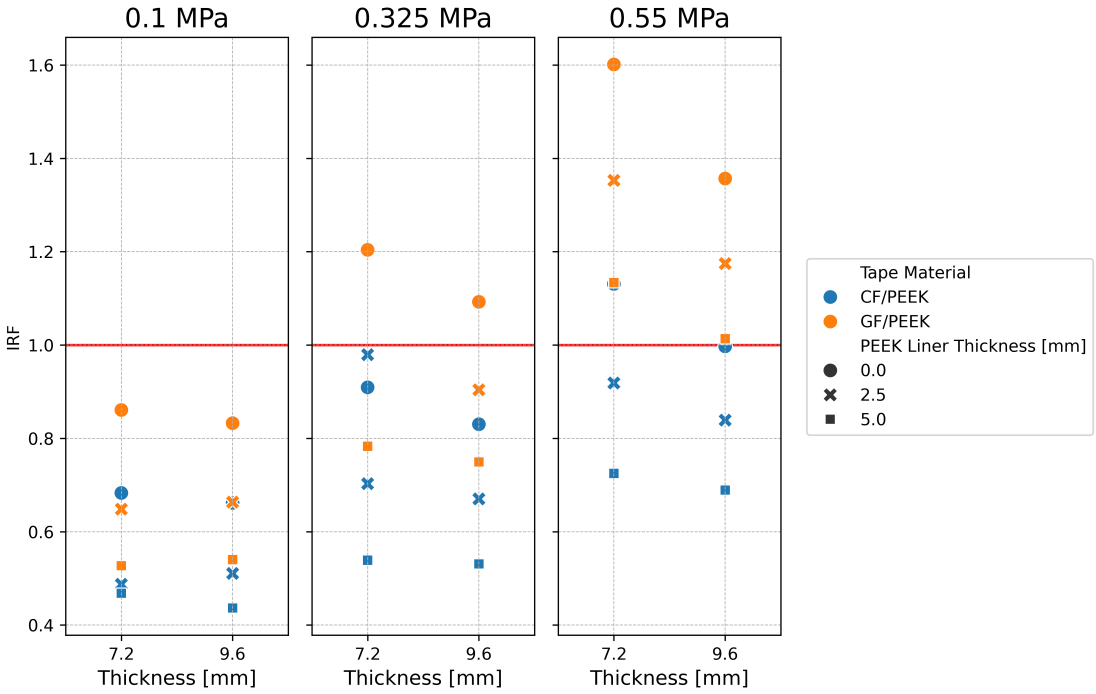

Figure 4.9: Failure of GF-PEEK and CF-PEEK comparison

GF-PEEK proves to be a worse candidate than CF except for some limit cases where the liner aids in failure performance. This is clearly ought by the lower modulus of the glass fiber, 90GPa, compared to the one of the carbon fiber, 230 GPa.

It is worth examining how the difference in fiber material influences the thermal performance of the tank, as this could inform the choice between Glass and Carbon fibers. Figure 4.10 illustrates the temperature distribution and the heat flux through the thickness for each specimen, while Table 4.1 lists the relevant material properties. The thickness coordinates in the figure start from the composite shell, so negative coordinates refer to the liner portion where present.

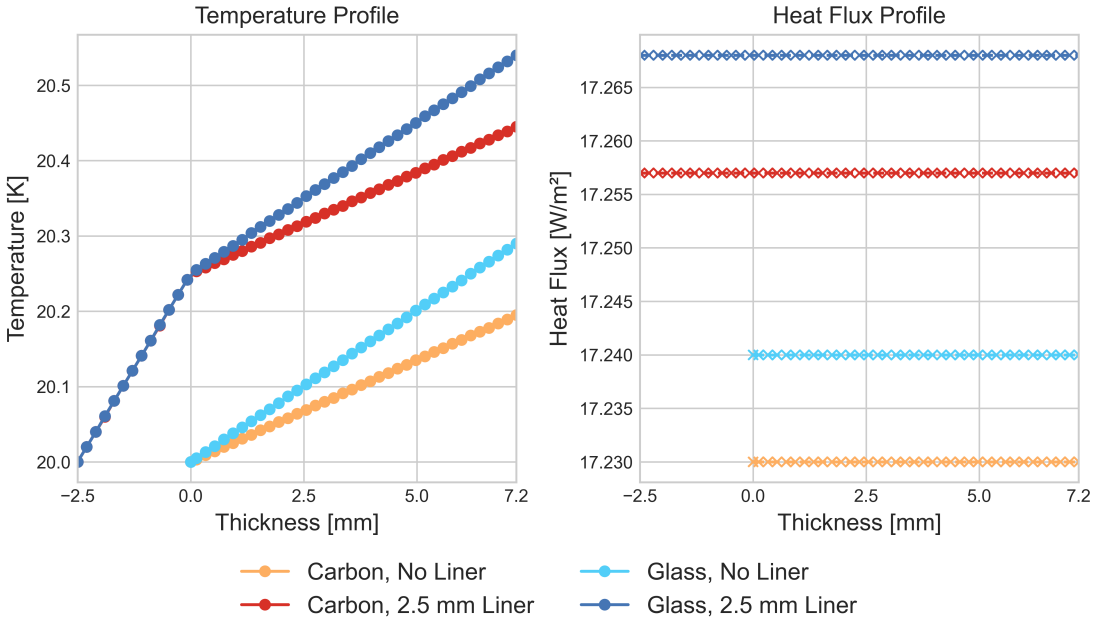

Figure 4.10: Thermal Comparison between Carbon and Glass fibers and PEEK matrix, for a 7.2 mm tank. PEEK was used as liner material and the liner thickness is 2.5 mm. For both carbon and glass fibers the liner results overlap along the liner thickness

Table 4.1: Thermal conductivities of the materials used in the analysis.

Material	**Direction**	**Thermal Conductivity [W/m/K]**
CF/PEEK	In-Plane	4.17
	Through-Thickness	0.64
GF/PEEK	In-Plane	0.67
	Through-Thickness	0.43
PEEK	Isotropic	0.17

As a consequence of the MLI layer used in the analysis (emissivity of 0.04), the overall thermal gradient between the inner and outer walls is not significant in any

of the cases. The highest temperature difference is approximately 0.1 K on the outer wall.

The variation in the temperature profiles is due to the different thermal conductivities of the materials. For a given heat flux, a material with lower thermal conductivity will exhibit a steeper temperature gradient. Conversely, a material with higher conductivity will have a flatter profile. As seen in the figure, the carbon fiber (CF/PEEK) curves are flatter than the glass fiber (GF/PEEK) curves, correctly indicating that CF/PEEK has a higher thermal conductivity. The effect of the PEEK liner is also clearly visible as its steep temperature profile confirms that the unfilled polymer has a significantly lower thermal conductivity than the fiber-reinforced composites.

Given the low thermal gradient, the mechanical properties of the materials are not significantly affected by temperature. It is therefore useful to investigate the difference in heat flux between the inner and outer walls, as its minimization is a critical aspect of thermal design. The results show that the linerless CF/PEEK tank exhibits a heat flow of 17.230 W/m^2, compared to 17.240 W/m^2 for the linerless GF/PEEK tank. The presence of the liner increases it compared to the unlined CF/PEEK tank, with final values of 17.257 W/m^2 for the lined CF/PEEK tank and 17.266 W/m^2 for the lined GF/PEEK tank.

Ultimately, the differences in thermal performance between the configurations are minimal due to the effectiveness of the chosen insulation system. While these results are critical for a detailed boil-off analysis (which is outside the scope of this work), they suggest that other factors are more decisive for the overall design. Therefore, the focus will shift to evaluating the mechanical performance, where factors like failure data, mass, and gravimetric capacity provide a more robust basis for selecting the optimal configuration.

4.3 Failure Performance Overview

From all the previous analyses, an overview of the best performing configuration has been done. The choice of the configurations has been made aiming to stay in a range of IRF values between 0.77 and 1.1. To provide a better overview of all materials, the two best performers, CF-PEEK and CF-PPS, the extended matrix liner, HDPE liner and linerless configuration were taken, while for GF-PEEK and CF-PA6 only the best performing values were included. Regarding the latter, although it doesn't fill in the chosen IRF range, it has been maintained to provide a way to visualise where PA6 positioned among the others. Additionally, for CF-PPS and CF-PEEK only, the configurations with the 2.5mm liner were chosen as they avoid unnecessary overdesign caused by and IRF below 0.7.

Fiber	**Matrix**	**Thickness [mm]**	**Liner Material**	**Liner Thickness [mm]**	**IRF**
CF	PPS	9,6	PPS	2,5	0,7234
CF	PPS	9,6	HDPE	2,5	0,7521
CF	PPS	9,6	LINERLESS	0	0,7616
CF	PPS	7,2	PPS	2,5	0,8336
CF	PEEK	9,6	PEEK	2,5	0,8390
CF	PPS	7,2	LINERLESS	0	0,8869
CF	PPS	7,2	HDPE	2,5	0,8990
CF	PEEK	7,2	PEEK	2,5	0,9186
CF	PEEK	9,6	HDPE	2,5	0,9731
CF	PEEK	9,6	LINERLESS	0	0,9971
GF	PEEK	9,6	PEEK	5	1,0134
CF	PA6	9,6	HDPE	5	1,3924
CF	PA6	9,6	PA6	5	1,4357

Table 4.2: Failure Performance Overview

4.4 Mass Analysis

As the influence of thickness and Pressure are of immediate comprehension, it is interesting to evaluate how the presence of a liner influences the tank performance, starting with how its mass, an important parameter to take into account, varies.

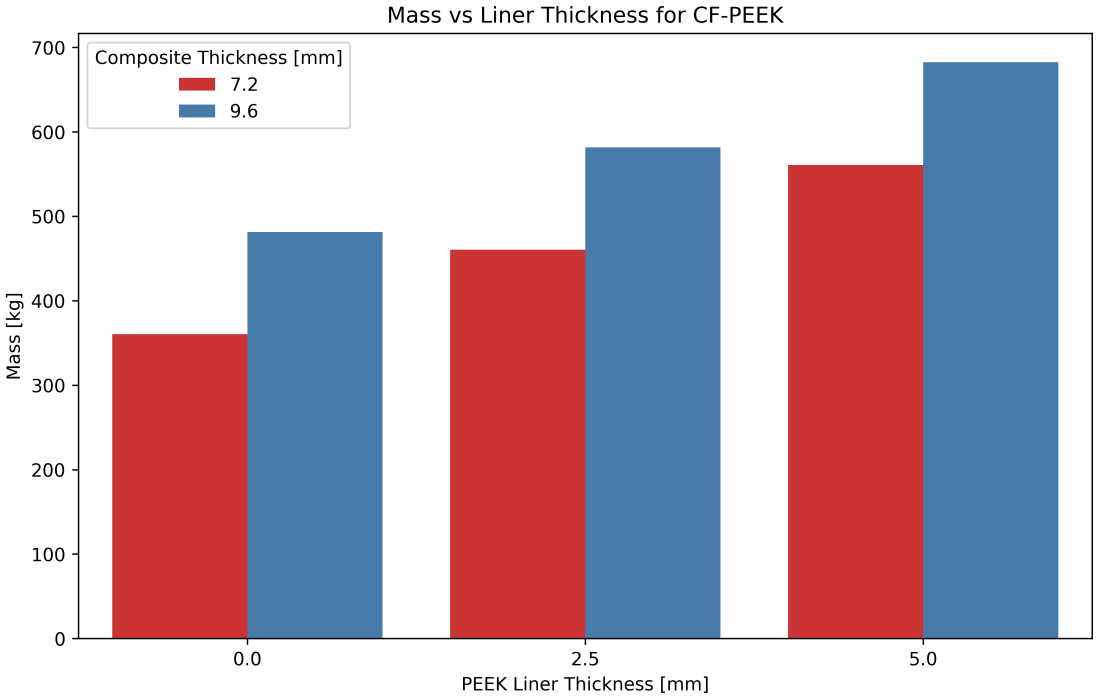

Figure 4.11: CF-PEEK Tank Mass variation

As one might expect, the presence of a PEEK liner increases the tank's mass, even though the effect of the composite thickness is dominant.

A significant modification is given by varying the length of the tank, thus its geometry. A 1 meter long tank has been taken into account and compared with the 3m one analysed until now. Failure assessment result yielded similar result and not a significant variation of the failure indexes, see appendix for the results of the failure assessment.

As the Parameters shown before bring to the same conclusion for both geometries, Tank Mass and Gravimetric Density proved to be a better mean to show the difference in performance between the two, the analysis results are illustrated in Figures 4.12 and 4.13.

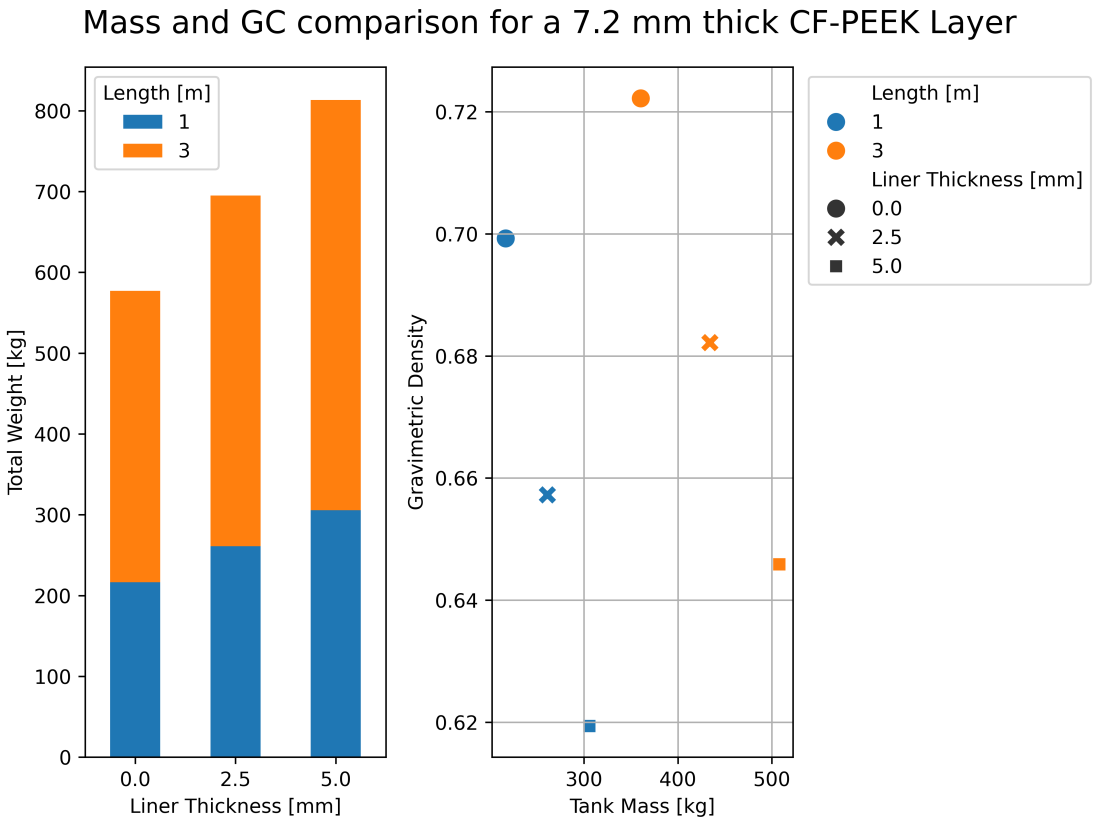

Figure 4.12: Mass and GC difference between the two geometries for a 7.2 mm thick CF-PEEK tank, Extended Matrix Liner

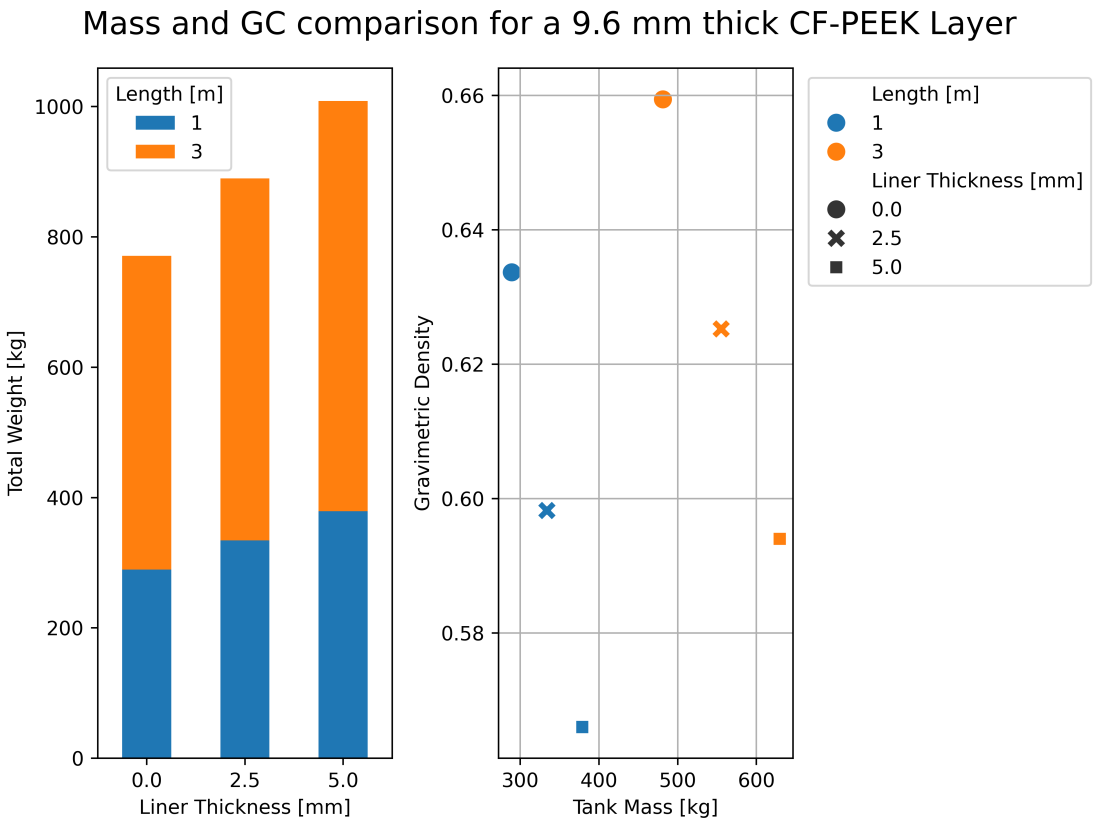

Figure 4.13: Mass and GC difference between the two geometries for a 9.6 mm thick CF-PEEK tank, Extended Matrix Liner

The best configurations that were identified in table 4.2 were reconsidered in the table below and compared to the same cases for the new geometry. Whereas for the previous cases the failure was the main object of comparison. This time the focus shifted on mass and gravimetric capacity. For the sake of simplicity the configurations were written into the table following the formula *[FIBER-MATRIX-THICKNESS-LINER-LINER THICKNESS]*.

Configuration	**IRF**	**Mass [kg]**	**Gravimetric Capacity**	**IRF**	**Mass [kg]**	**Gravimetric Capacity**
	3m			**1m**		
CF-PPS-7.2-LINERLESS	0,887	364,13	0,72	0,934	205,72	0,71
CF-PPS-7.2-HDPE-2.5	0,899	437,72	0,68	0,946	247,30	0,67
CF-PEEK-7.2-PEEK-2.5	0,919	460,42	0,67	0,967	260,13	0,66
CF-PPS-7.2-PPS-2.5	0,834	471,11	0,66	0,878	266,17	0,66
CF-PEEK-9.6-LINERLESS	0,997	481,41	0,66	0,999	289,39	0,63
CF-PPS-9.6-LINERLESS	0,762	486,24	0,66	0,766	292,30	0,63
CF-PEEK-9.6-HDPE-2.5	0,973	555,37	0,63	0,987	334,01	0,60
CF-PPS-9.6-HDPE-2.5	0,752	560,22	0,62	0,756	336,93	0,60
CF-PEEK-9.6-PEEK-2.5	0,839	581,71	0,61	0,883	328,65	0,61
CF-PPS-9.6-PPS-2.5	0,723	593,62	0,61	0,761	335,38	0,60

Table 4.3: Configurations Overview for Different Geometries, sorted by Mass for the 3 m geometry

As one can observe, the varied geometry doesn't influence in a significant way how the configurations behave in terms of inverse reserve factor and gravimetric capacity. The latter happens because the reduction in length of the tank yields to a reduction of the total volume of both tank and hydrogen, wich keep approximately the same ratio as the first geometry, hence the similar values of GC. A different matter is the mass, as it is evident how the smaller tank gives a good reduction in mass, enabling for the use of the configurations in cases where dimensions matter the most.

To provide a quick way to visualize which one is the best configuration, each configuration Mass, IRF and GC ha been assembled in the defined Performance Index and their difference for both geometries hereby presented.

	Performance Index F	
Configuration	**3m**	**1m**
CF-PPS-7.2-LINERLESS	0.74	0.64
CF-PPS-9.6-LINERLESS	0.56	0.46
CF-PPS-7.2-PPS-2.5	0.54	0.52
CF-PPS-7.2-HDPE-2.5	0.54	0.46
CF-PEEK-7.2-PEEK-2.5	0.45	0.35
CF-PPS-9.6-HDPE-2.5	0.25	0.00
CF-PEEK-9.6-HDPE-2.5	0.13	0.03
CF-PEEK-9.6-PEEK-2.5	0.11	0.15
CF-PPS-9.6-PPS-2.5	0.00	0.09
CF-PEEK-9.6-LINERLESS	0.00	0.00

Table 4.4: Performance Index Configurations Overview

The best configuration is the 7.2 mm CF-PPS linerless tank for both geometries, this is because it has the best tradeoff between IRF, Mass and GC. It is then followed by different combinations of CF-PPS and CF-PEEK with an HDPE Liner, which have similiar performances, with a Performance Index approximately 30% lower. The rest of the configurations yielded values close to 0, this is ought to them having a high mass, low GC or high IRF, which drive the performance index towards 0.

Chapter 5

Discussion

The study evidenced the difference between various materials in how they are able to withstand failure at cryogenic temperatures for a liquid hydrogen storage application. The variation of all parameters allowed the visualization of how each of those impacts the performance of the tank. By increasing the thickness, the tank performs better with lower values of the Inverse Reserve Factor. Adding a Liner helps further, rending feasible the use of configurations otherwise at a disadvantage. Although, A tradeoff between all the parameters is needed. In fact the results showed how choosing the higher values of liner and composite thickness isn't always the best choice, as it comes with a significative increase in mass, thus lowering the efficiency of the tank. While all of these qualities could be analyzed and discussed upon, the study can see use of a wide range of improvements.

First of all the quality of the data should be reviewed, as the impossibility to find a comprehensive dataset of material properties at cryogenic temperatures made it mandatory to interpolate the properties of the majority of the materials taken into exam. The ideal solution would be to test each materials in a lab and use the resulting data, providing with a better accuracy.

Regarding the model, spherical caps have been used. This solution was chosen for simplicity of simulation, a refinement of the caps section of the tank should be done for more accurate results. Consequentially, as a standard tank needs to be refilled, thus to have an opening, a boss should be added to the model and its interaction with the composite material investigated to have a better understanding of how another component of a tank interacts with the composite layer.

Further expanding on the matter, as a consequence of the scarceness of data, a better and more complete temperature model should be considered.

As the study itself focused on delineating the main differences between materials, all the other design aspects were neglected, as the modeling of a proper insulation layer and different analyses on permeability and crack propagation. As permeability is a crucial factor in the performance of a liquid hydrogen storage tank, a

simulation should be taken into account. Furthermore, as a common application sees the emptying and refilling of the tank for a number of cycles, a simulation to investigate the behavior of the materials under a continuous cycle on a wide range of temperatures could give more insights and improve the quality of the results.

Finally, the analysis incorporated a conservative approach accounting for neglected factors by applying a high safety factor of 2.75 to the functional pressure to determine the design load. This conservative approach resulted in an overestimation of the mass and subsequently an underestimation of the gravimetric capacity. This leaves significant room for optimization and further investigation into the feasibility of configurations that were initially deemed less favorable.

Chapter 6

Conclusions

The analyses conducted in this study reveal results that are consistent with the expected behavior of cylindrical structures. The first results showed how increasing the thickness of the composite shell was shown to reduce the IRF, mitigating failure. At the same time, a design load was defined, starting from the functioning pressure of 0.2MPa and multiplying by a generous safety factor of 2.75, the resulting pressure of 0.55MPa was chosen as design load to base the successive analyses upon. Among the materials evaluated, CF/PPS and CF/PEEK demonstrated the best performance, followed by CF/PA6 and CF/LM-PAEK. The latter was outshadowed by the alternatives, which were further analysed. Optimal thickness values for the composite shell were identified as 7.2mm and 9.6mm, aiming for a balance between mass minimization and the right value of IRF. At the same time, the effect of a liner has been investigated, showing the utility of the liner itself in failure mitigation, although resulting in a mass increase. Both HDPE and and Extended Matrix Liner were studied, with the latter proving to be better especially for PEEK, which benefited the most thanks to its superior properties compared to HDPE. In contrast, the variation of the fiber material with glass fibers did not yield improved results, given the better mechanical properties of carbon fibers and the thermal performance differences were negligible for the studied cases, moving the focus on the evaluation of other factors such as IRF, Mass and Gravimetric Capacity. Likewise, the variation in length of the cylindrical section of the structure did not evidence significant differences in the results of the IRF, except for the difference in the overall mass of the structure. To better compare all the configurations taken into exam, a performance index was built, by weighting the contribute of the three main group of results, IRF, Mass and Gravimetric Capacity. As all of them are significant variables in the design of the tank, they were weighted equally.

The analysis of this index revealed that the 7.2 mm linerless CF-PPS tank is the premier configuration for both the 1m and 3m geometries. This design offers the best trade-off between a safe IRF value, minimal mass, and the highest gravimetric

capacity with a performance index of 0.74 for the 3 m long tank and 0.64 for the 1 m long one. It was followed by the 9.6 mm linerless CF-PPS configuration and various CF-PEEK configurations which also stand as viable, high-performing options depending on specific mission requirements, demonstrating performance indices ranging from 0.45 to 0.56 for both geometries.

This study provided valuable insights and facilitated a clear comparison between different composite materials, highlighting optimal configurations for further investigation. Despite the positive outcomes, the study employed a simplified approach, suggesting ample opportunities for improvement. These include enhancing data accuracy, refining thermal models, and expanding the range of materials and configurations considered. The conservative safety factor applied potentially led to an overestimation of mass and an underestimation of gravimetric capacity, indicating potential areas for future refinement.

Overall, the findings of the study lay a foundation for future research, offering insights and directions for further investigations regarding the analysis of Composite applications at Cryogenic Properties.

Appendix A

Material Model

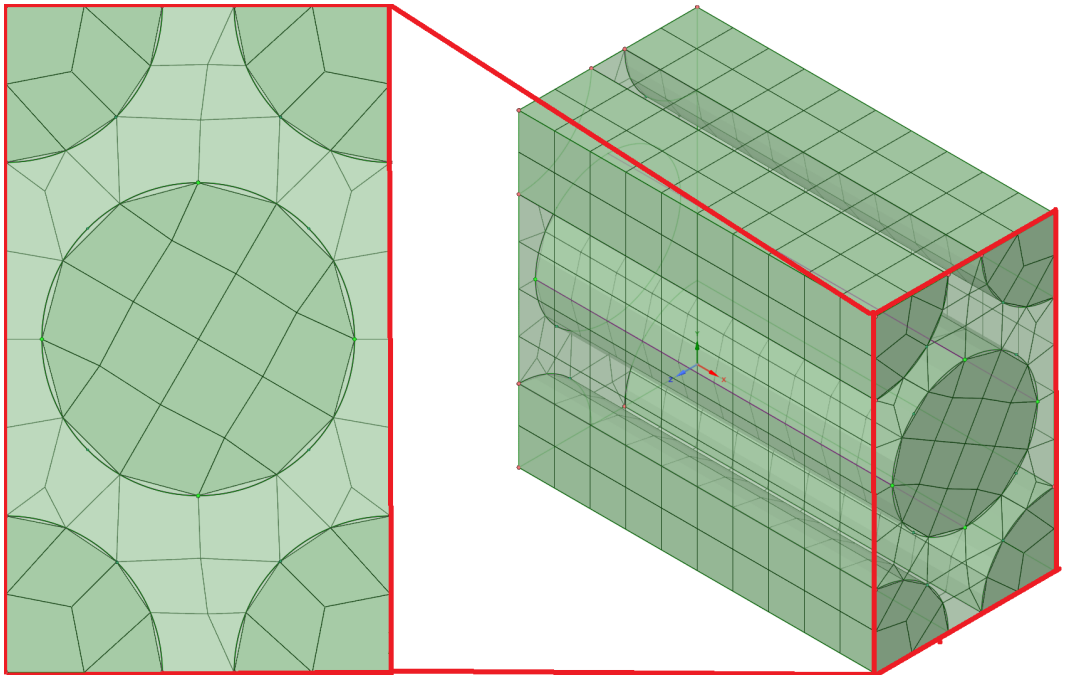

Figure A.1: Representative Volume Element (RVE) model used for the simulation of the composite materials properties

Table A.1: Composite ANSYS Material Properties

Property	**CF/PEEK**	**CF/PA6**	**CF/PPS**	**CF/LM-PAEK**	**GF/PEEK**
Density [kg/m^3]	1592	1528	1608	1644	2004
CTE [1/K]					
X	-4.60×10^{-7}	-6.00×10^{-7}	-5.22×10^{-7}	-1.23×10^{-7}	6.45×10^{-6}
Y	4.38×10^{-6}	2.93×10^{-6}	3.43×10^{-6}	4.44×10^{-6}	1.70×10^{-5}
Z	4.38×10^{-6}	2.93×10^{-6}	3.43×10^{-6}	4.44×10^{-6}	1.70×10^{-5}
Tensile Modulus [GPa]					
X	168.00	165.00	167.00	173.00	56.40
Y	22.60	7.60	19.40	75.00	20.90
Z	22.6	7.6	19.4	75	20.9
Poisson Ratio					
XY	0.3	0.27	0.31	0.34	0.28
YZ	0.38	0.27	0.45	0.55	0.43
XZ	0.3	0.27	0.31	0.34	0.27
Shear Modulus [GPa]					
XY	8.6	3.43	6.64	2.2	7.28
YZ	8.2	2.97	6.75	2.5	7.36
XZ	8.6	3.43	6.64	2.2	7.28
Tensile Strength [MPa]					
X	2400	1050	1799	2410	178
Y	86	67	43.5	86	14
Z	86	67	43.5	86	14
Compressive Strength [MPa]					
X	1300	1000	777	1300	168
Y	86	67	44	85	14
Z	86	67	44	85	14
Shear Strength [MPa]					
XY	152	50	95	42	77
YZ	152	50	95	42	77
XZ	152	50	95	42	77
Thermal Conductivity [W/m/K]					
X	4.16	4.21	4.17	4.62	0.66
Y	0.64	1	0.72	3.1	0.4
Z	0.64	1	0.72	3.1	0.4

Table A.2: Fibers and Polymers Properties

Property	**PEEK**	**PPS**	**LM-PAEK**	**PA6**	**HDPE**	**IM7**	**S-Glass**
Density [kg/m^3]	1260	1350	1440	1150	924	2180	2500
CTE [1/K]	3.00×10^{-5}	8.00×10^{-6}	9.00×10^{-6}	9.00×10^{-6}	2.00×10^{-5}	-4.00×10^{-7}	2.90×10^{-6}
Tensile Modulus [GPa]	6.1	4.8	19.5	2.1	4.83	276	90
Poisson Ratio	0.3779	0.37	0.44	0.23	0.4	0.3	0.22
Yield Strength [MPa]	110	55.2	–	30	28.4	5.65	4.58
Thermal Conductivity [W/m/K]	0.173	0.2	1.3	0.29	0.5	5.4	1

Appendix B

Results - Different Liner Materials

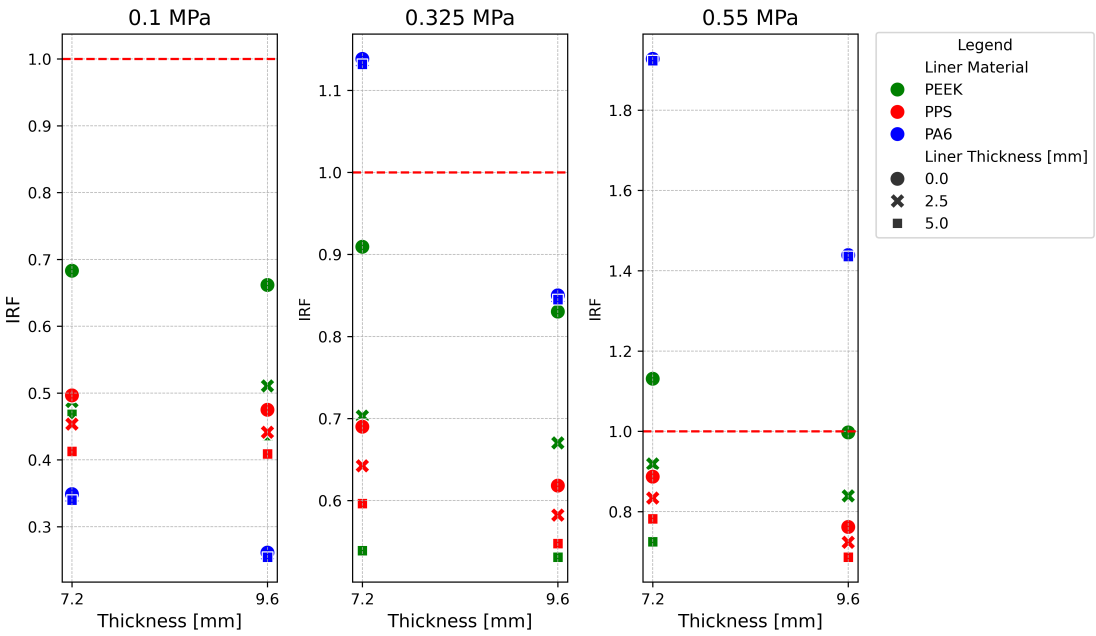

Figure B.1: Comparison of different liner materials for a CF-PEEK Tank

The plot evidences how the choice of the same material as the composite yields to a better performance, given also by the choice of PEEK which has better mechanical properties than the other polymers.

Appendix C

Results - Second Geometry Failure data

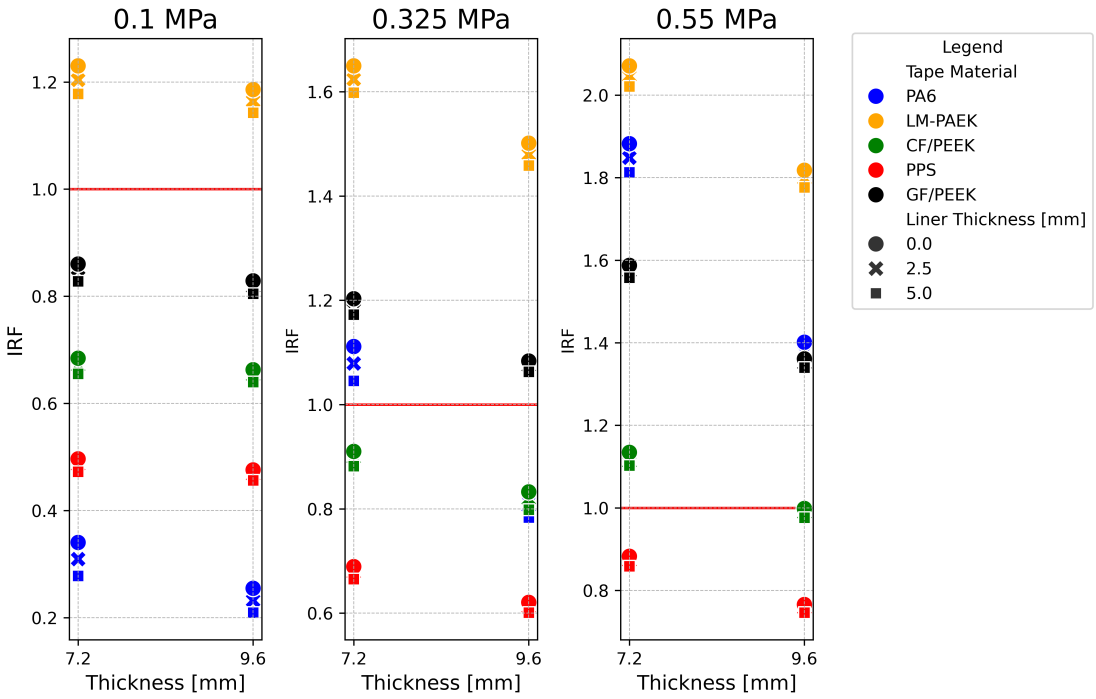

Figure C.1: Failure data for the 1 m long tank, presence of a HDPE Liner

For the 1 m cylindrical section Tank, the performance comments are in line with the previous analyses analyses.

Bibliography

[1] https://global.toyota/jp/newsroom/toyota/34276191.html (cit. on p. 2).

[2] https://www.airbus.com/en/innovation/low-carbon-aviation/hydrog (cit. on p. 3).

[3] https://www.nccuk.com/what-we-do/technologies/braiding/ (cit. on p. 10).

[4] https://www.hydrogen.energy.gov/docs/hydrogenprogramlibraries/pdfs/review17/st001_ahluwalia_2017_o.pdf?Status=Master (cit. on p. 21).

[5] https://www.material.be/composite-star/features/ (cit. on p. 36).

[6] R.K. Ahluwalia, T.Q. Hua, J.-K. Peng, S. Lasher, K. McKenney, J. Sinha, and M. Gardiner. «Technical Assessment Of Cryo-Compressed Hydrogen Storage Tank Systems For Automotive Applications». In: *International Journal of Hydrogen Energy* 35.9 (May 2010), pp. 4171–4184. ISSN: 0360-3199. DOI: 10.1016/j.ijhydene.2010.02.074 (cit. on p. 5).

[7] Alexander Air, Ebrahim Oromiehie, and B. Gangadhara Prusty. «Design And Manufacture Of A Type V Composite Pressure Vessel Using Automated Fibre Placement». In: *Composites Part B: Engineering* 266 (Nov. 2023), p. 111027. ISSN: 1359-8368. DOI: 10.1016/j.compositesb.2023.111027 (cit. on pp. 1, 6, 7, 10, 22).

[8] Alexander Air, Md Shamsuddoha, and B. Gangadhara Prusty. «A Review Of Type V Composite Pressure Vessels And Automated Fibre Placement Based Manufacturing». In: *Composites Part B: Engineering* 253 (Mar. 2023), p. 110573. ISSN: 1359-8368. DOI: 10.1016/j.compositesb.2023.110573 (cit. on pp. 7, 24).

[9] V. Alcantar, S.M. Aceves, E. Ledesma, S. Ledesma, and E. Aguilera. «Optimization Of Type 4 Composite Pressure Vessels Using Genetic Algorithms And Simulated Annealing». In: *International Journal of Hydrogen Energy* 42.24 (June 2017), pp. 15770–15781. DOI: 10.1016/j.ijhydene.2017.03.032 (cit. on pp. 1, 24).

[10] Mariana Pimenta Alves, Waseem Gul, Carlos Alberto Cimini Junior, and Sung Kyu Ha. «A Review On Industrial Perspectives And Challenges On Material, Manufacturing, Design And Development Of Compressed Hydrogen Storage Tanks For The Transportation Sector». In: *Energies* 15.14 (July 2022), p. 5152. ISSN: 1996-1073. DOI: 10.3390/en15145152 (cit. on pp. 1–3, 11, 12).

[11] Youcef Sid Amer, Samir Benammar, Kong Fah Tee, Mohammed Wadi, and Mohammed S. Jouda. «A Contribution To Structural Reliability Analysis Of Composite High-Pressure Hydrogen Storage Tanks». In: *Journal of Konbin* 53.2 (June 2023), pp. 33–44. DOI: 10.5604/01.3001.0053.7104 (cit. on p. 24).

[12] Steven Arnold, Brett Bednarcyk, Craig Collier, and Phillip Yarrington. «Spherical Cryogenic Hydrogen Tank Preliminary Design Trade Studies». In: *48th AIAA/ASME/ASCE/AHS/ASC Structures, Structural Dynamics, and Materials Conference*. American Institute of Aeronautics and Astronautics, Apr. 2007. DOI: 10.2514/6.2007-2290 (cit. on pp. 24, 30).

[13] Mohammad Azeem et al. «Application Of Filament Winding Technology In Composite Pressure Vessels And Challenges: A Review». In: *Journal of Energy Storage* 49 (May 2022), p. 103468. ISSN: 2352-152X. DOI: 10.1016/j.est.2021.103468 (cit. on pp. 7, 9).

[14] H. Barthelemy, M. Weber, and F. Barbier. «Hydrogen Storage: Recent Improvements And Industrial Perspectives». In: *International Journal of Hydrogen Energy* 42.11 (Mar. 2017), pp. 7254–7262. ISSN: 0360-3199. DOI: 10.1016/j.ijhydene.2016.03.178 (cit. on p. 6).

[15] P. Blanc-Vannet, P. Papin, M. Weber, P. Renault, J. Pepin, E. Lainé, G. Tantchou, S. Castagnet, and J.-C. Grandidier. «Sample Scale Testing Method To Prevent Collapse Of Plastic Liners In Composite Pressure Vessels». In: *International Journal of Hydrogen Energy* 44.17 (Apr. 2019), pp. 8682–8691. ISSN: 0360-3199. DOI: 10.1016/j.ijhydene.2018.10.031 (cit. on p. 24).

[16] A. Boretti. «Progress in cold/cryo-pressurized composite tanks for hydrogen». In: *MRS Communications* 13 (2023), pp. 400–405. DOI: 10.1557/s43579-023-00379-6 (cit. on p. 11).

[17] Samir Borriello. «Analisi Dei Processi Produttivi Di Serbatoi In Composito Per Lo Stoccaggio Di Idrogeno Gassoso Ad Alta Pressione E Sviluppo Di Un Modello Agli Elementi Finiti Per La Previsione Della Pressione Di Scoppio». In: (2018). URL: https://tesi.univpm.it/retrieve/16b2caa5-d72d-40a3-be6f-c24b407e452d/Tesi%20magistrale%20SamirBorriello.pdf (cit. on p. 30).

[18] Lyazid Bouhala et al. «Advancement in the Modeling and Design of Composite Pressure Vessels for Hydrogen Storage: A Comprehensive Review». In: *Journal of Composites Science* 8.9 (Aug. 2024), p. 339. ISSN: 2504-477X. DOI: 10.3390/jcs8090339 (cit. on p. 20).

[19] G BREWER. «The Prospects For Liquid Hydrogen Fueled Aircraft». In: *International Journal of Hydrogen Energy* 7.1 (1982), pp. 21–41. ISSN: 0360-3199. DOI: 10.1016/0360-3199(82)90205-1 (cit. on p. 5).

[20] Davide Camplese, Giordano Emrys Scarponi, Carmela Chianese, Aliasghar Hajhariri, Robert Eberwein, Frank Otremba, and Valerio Cozzani. «Modeling the performance of multilayer insulation in cryogenic tanks undergoing external fire scenarios». In: *Process Safety and Environmental Protection* 186 (June 2024), pp. 1169–1182. ISSN: 0957-5820. DOI: 10.1016/j.psep.2024.04.061 (cit. on p. 34).

[21] D. Cecere, E. Giacomazzi, and A. Ingenito. «A Review On Hydrogen Industrial Aerospace Applications». In: *International Journal of Hydrogen Energy* 39.20 (July 2014), pp. 10731–10747. ISSN: 0360-3199. DOI: 10.1016/j.ijhydene.2014.04.126 (cit. on p. 1).

[22] Ashley Chadwick. «Composite Tanks For Hydrogen Storage». 2023 (cit. on p. 6).

[23] Zhen-Kun Chen, Jiao-Ping Yang, Qing-Qing Ni, Shao-Yun Fu, and Yong-Gang Huang. «Reinforcement of epoxy resins with multi-walled carbon nanotubes for enhancing cryogenic mechanical properties». In: *Polymer* 50.19 (Sept. 2009), pp. 4753–4759. ISSN: 0032-3861. DOI: 10.1016/j.polymer.2009.08.001 (cit. on p. 12).

[24] Qian Cheng, Ruiqiang Zhang, Zhusheng Shi, and Jianguo Lin. «Review of common hydrogen storage tanks and current manufacturing methods for aluminium alloy tank liners». In: *International Journal of Lightweight Materials and Manufacture* 7.2 (Mar. 2024), pp. 269–284. ISSN: 2588-8404. DOI: 10.1016/j.ijlmm.2023.08.002 (cit. on p. 21).

[25] Xiangrong Cheng, Bing Du, Jia He, Wanling Long, Guiyang Su, Jingwei Liu, Zhenhua Fan, and Liming Chen. «A review of thermoplastic composites on wind turbine blades». In: *Composites Part B: Engineering* 299 (June 2025), p. 112411. ISSN: 1359-8368. DOI: 10.1016/j.compositesb.2025.112411 (cit. on p. 11).

[26] X. Chu, Zuheng Wu, Rui Huang, Yongqiang Zhou, and Laifeng Li. «Mechanical And Thermal Expansion Properties Of Glass Fibers Reinforced Peek Composites At Cryogenic Temperatures». In: (2010). DOI: 10.1016/J.CRYOGENICS.2009.12.003. URL: https://www.semanticscholar.org/paper/0aa236fd933cb4d17278f9fa6994b9cdc0d60456 (cit. on pp. 12, 32).

[27] D.J. Durbin and C. Malardier-Jugroot. «Review Of Hydrogen Storage Techniques For on board Vehicle Applications». In: *International Journal of Hydrogen Energy* 38.34 (Nov. 2013), pp. 14595–14617. ISSN: 0360-3199. DOI: 10.1016/j.ijhydene.2013.07.058 (cit. on p. 4).

[28] Michael Ebermann, Raffael Bogenfeld, Janko Kreikemeier, and Rainer Glüge. «Analytical And Numerical Approach To Determine Effective Diffusion Coefficients For Composite Pressure Vessels». In: *Composite Structures* 291 (July 2022), p. 115616. ISSN: 0263-8223. DOI: 10.1016/j.compstruct.2022.115616 (cit. on p. 24).

[29] Qingping Feng, Jiaoping Yang, Yu Liu, Hongmei Xiao, and Shaoyun Fu. «Simultaneously Enhanced Cryogenic Tensile Strength, Ductility and Impact Resistance of Epoxy Resins by Polyethylene Glycol». In: *Journal of Materials Science & Technology* 30.1 (Jan. 2014), pp. 90–96. ISSN: 1005-0302. DOI: 10.1016/j.jmst.2013.08.016 (cit. on p. 12).

[30] Hayato Fukui, Akinori Yoshimura, and Ryosuke Matsuzaki. «Structural Optimization For Cfrp Cryogenic Tank Based On Energy Release Rate». In: *Composite Structures* 152 (Sept. 2016), pp. 883–890. ISSN: 0263-8223. DOI: 10.1016/j.compstruct.2016.06.004 (cit. on pp. 22, 24).

[31] Julián A. Gómez and Diogo M. F. Santos. «The Status Of On-Board Hydrogen Storage In Fuel Cell Electric Vehicles». In: 2023. DOI: doi.org/10.3390/designs7040097 (cit. on pp. 1, 4, 21).

[32] Paulo Teixeira Goncalves, Albertino Arteiro, and Nuno Rocha. «Experimental Characterization And Numerical Analysis Of Cfrps At Cryogenic Temperatures». In: *International Journal of Mechanical Sciences* 265 (Mar. 2024), p. 108899. ISSN: 0020-7403. DOI: 10.1016/j.ijmecsci.2023.108899 (cit. on p. 12).

[33] D. M. Grogan, S. B. Leen, C. O. A. Semprimoschnig, and C. M. Ó Brádaigh. «Damage Characterisation Of Cryogenically Cycled Carbon Fibre/peek Laminates». In: 66 (2014), pp. 237–250. ISSN: 1359-835X. DOI: 10.1016/j.compositesa.2014.08.007 (cit. on pp. 30, 31).

[34] D.M. Grogan, C.M. Ó Brádaigh, J.P. McGarry, and S.B. Leen. «Damage And Permeability In Tape-Laid Thermoplastic Composite Cryogenic Tanks». In: *Composites Part A: Applied Science and Manufacturing* 78 (Nov. 2015), pp. 390–402. DOI: 10.1016/j.compositesa.2015.08.037 (cit. on pp. 21, 22, 24).

[35] Waseem Gul, Yu En Xia, Pierre Gérard, and Sung Kyu Ha. «Characterization of Polymeric Composites for Hydrogen Tank». In: *Polymers* 15 (2023). DOI: 10.3390/polym15183716 (cit. on pp. 11, 12).

[36] Lee Harper and Mike Clifford, eds. *Design And Manufacture Of Structural Composites*. First edition. Woodhead Publishing series in composites science and engineering. Cambridge, MA: Woodhead Publishing, an imprint of Elsevier, 2023. 1 p. ISBN: 978-0-12-819160-6 (cit. on p. 10).

[37] Chaoming He, Y. Rong, Haoran Sun, and Chen Zilong. «Lightweight Multilayer Composite Structure For Hydrogen Storage Tank». In: (2016). DOI: 10.1016/J.IJHYDENE.2016.04.184. URL: https://www.semanticscholar.org/paper/57f6bbb2341d9caeeb9a47a590bcbeebaf652c92 (cit. on p. 24).

[38] Yuxin He, Song Yang, Hu Liu, Qian Shao, Qiuyu Chen, Chang Lu, Yuanli Jiang, Chuntai Liu, and Zhanhu Guo. «Reinforced carbon fiber laminates with oriented carbon nanotube epoxy nanocomposites: Magnetic field assisted alignment and cryogenic temperature mechanical properties». In: *Journal of Colloid and Interface Science* 517 (May 2018), pp. 40–51. ISSN: 0021-9797. DOI: 10.1016/j.jcis.2018.01.087 (cit. on p. 12).

[39] Jörg Hohe, Achim Neubrand, Sascha Fliegener, Carla Beckmann, Michael Schober, Klaus-Peter Weiss, and Simon Appel. «Performance Of Fiber Reinforced Materials Under Cryogenic Conditions—A Review». In: *Composites Part A: Applied Science and Manufacturing* 141.epoxy (Feb. 2021), p. 106226. ISSN: 1359-835X. DOI: 10.1016/j.compositesa.2020.106226 (cit. on p. 32).

[40] Cheng Huang, MingFa Ren, Tong Li, Xin Chang, Jie Cong, and YongJun Lei. «Trans-Scale Modeling Framework For Failure Analysis Of Cryogenic Composite Tanks». In: *Composites Part B: Engineering* 85 (Feb. 2016), pp. 41–49. ISSN: 1359-8368. DOI: 10.1016/j.compositesb.2015.09.023 (cit. on pp. 22, 24).

[41] Yonghua Huang, Bin Wang, Shaohua Zhou, Jingyi Wu, Gang Lei, Peng Li, and Peijie Sun. «Modeling and experimental study on combination of foam and variable density multilayer insulation for cryogen storage». In: *Energy* 123 (Mar. 2017), pp. 487–498. ISSN: 0360-5442. DOI: 10.1016/j.energy.2017.01.147 (cit. on p. 34).

[42] Susheel Kalia and Shao-Yun Fu, eds. *Polymers At Cryogenic Temperatures*. Springer Berlin Heidelberg, 2013. DOI: 10.1007/978-3-642-35335-2 (cit. on p. 32).

[43] Bahaa Kamel, Mohamed El-Anwar, and Nihad El-Chazly. «Design of Hydrogen Storage Tanks Fabricated from Composite Materials». In: May 2014 (cit. on p. 20).

[44] S. Kanagaraj. «Thermal Expansion Of Glass Fabric-Epoxy Composites At Cryogenic Temperatures». In: *AIP Conference Proceedings*. Vol. 711. AIP, 2004, pp. 201–208. DOI: 10.1063/1.1774570 (cit. on p. 32).

[45] Daehoon Kang, Sungho Yun, and Bo-kyong Kim. «Review Of The Liquid Hydrogen Storage Tank And Insulation System For The High-Power Locomotive». In: *Energies* 15.12 (June 2022), p. 4357. ISSN: 1996-1073. DOI: 10.3390/en15124357 (cit. on p. 3).

[46] Anass Kheir, Hamid Mounir, Zakaria Lafdaili, Omar Rajad, and Ismail Lagrat. «Modeling And Analysis Of Laminate Structures Of A Pressurized Hydrogen Tank». In: *E3S Web of Conferences* 469 (2023). Ed. by B. Benhala, A. Raihani, B. Boukili, A. Sallem, and M. Qbadou, p. 00022. ISSN: 2267-1242. DOI: 10.1051/e3sconf/202346900022 (cit. on p. 24).

[47] Myung-Sung Kim and Kang Woo Chun. «A Comprehensive Review on Material Compatibility and Safety Standards for Liquid Hydrogen Cargo and Fuel Containment Systems in Marine Applications». In: *Journal of Marine Science and Engineering* 11.10 (Oct. 2023), p. 1927. ISSN: 2077-1312. DOI: 10.3390/jmse11101927 (cit. on p. 5).

[48] Manfred Klell. *Storage of Hydrogen in the Pure Form*. Mar. 2010. DOI: 10.1002/9783527629800.ch1 (cit. on p. 5).

[49] Hisashi Kumazawa, Hirotaka Hayashi, Ippei Susuki, and Takao Utsunomiya. «Damage and permeability evolution in CFRP cross-ply laminates». In: *Composite Structures* 76.1–2 (Oct. 2006), pp. 73–81. ISSN: 0263-8223. DOI: 10.1016/j.compstruct.2006.06.011 (cit. on pp. 21, 22).

[50] Henrietta W. Langmi, Nicolaas Engelbrecht, Phillimon M. Modisha, and Dmitri Bessarabov. «Hydrogen Storage». In: *Electrochemical Power Sources: Fundamentals, Systems, and Applications*. Elsevier, 2022, pp. 455–486. ISBN: 9780128194249. DOI: 10.1016/b978-0-12-819424-9.00006-9 (cit. on p. 5).

[51] Nieves Lapeña-Rey, Jonay Mosquera, Elena Bataller, and Fortunato Ortí. «First Fuel-Cell Manned Aircraft». In: *Journal of Aircraft* 47.6 (Nov. 2010), pp. 1825–1835. ISSN: 1533-3868. DOI: 10.2514/1.42234 (cit. on p. 3).

[52] Michael;Multhoff Jörg Lengersdorf. «Iccm 20 Evaluation Of Braiding As A Method For The Manufacutring Of Composite Pressure Vessels». In: *20th International Conference on Composite Materials*. 5207 (cit. on pp. 9, 10).

[53] Haoran Liu, Changjian Wang, Bing Chen, and Zhi Zhang. «A further study of pyrolysis of carbon fibre-epoxy composite from hydrogen tank: Search optimization for kinetic parameters via a Shuffled Complex Evolution.» In: *Journal of hazardous materials* 374 (2019), pp. 20–25. DOI: 10.1016/j.jhazmat.2019.03.100 (cit. on p. 22).

[54] Yuesen Liu, Jiuming Xie, Xin Chen, Jiawen Zhang, Meiqing Wan, Zengxi Sun, and Chunlin Yang. «Characterization of progressive damage behaviour and failure mechanism of carbon fiber reinforced composite laminates». In: *Scientific Reports* 15.1 (Apr. 2025). ISSN: 2045-2322. DOI: 10.1038/s41598-025-98774-7 (cit. on p. 22).

[55] Zai Liu, Weiwei Hui, Guoqing Chen, and Peng Cao. «Multiscale analyses of the damage of composite rocket motor cases». In: *Frontiers in Materials* 10 (June 2023). ISSN: 2296-8016. DOI: 10.3389/fmats.2023.1198493 (cit. on p. 20).

[56] Sofoklis S. Makridis. «Hydrogen Storage And Compression». In: *Methane and Hydrogen for Energy Storage*. Institution of Engineering and Technology, July 2016, pp. 1–28. ISBN: 9781785611940. DOI: 10.48550/arXiv.1702.06015 (cit. on p. 24).

[57] Garrett W Melenka and Cagri Ayranci. «Advanced Measurement Techniques For Braided Composite Structures: A Review Of Current And Upcoming Trends». In: *Journal of Composite Materials* 54.25 (Apr. 2020), pp. 3895–3917. ISSN: 1530-793X. DOI: 10.1177/0021998320903105 (cit. on p. 10).

[58] Subodh K Mital, John Z Gyekenyesi, Steven M Arnold, Roy M Sullivan, Jane M Manderscheid, and Pappu LN Murthy. «Review Of Current State Of The Art And Key Design Issues With Potential Solutions For Liquid Hydrogen Cryogenic Storage Tank Structures For Aircraft Applications». In: (2006) (cit. on p. 24).

[59] R. Morales-Ospino, A. Celzard, and V. Fierro. «Strategies to recover and minimize boil-off losses during liquid hydrogen storage». In: *Renewable and Sustainable Energy Reviews* 182 (Aug. 2023), p. 113360. ISSN: 1364-0321. DOI: 10.1016/j.rser.2023.113360 (cit. on pp. 5, 8).

[60] Ines Mössinger, Lukas Raps, Daniel Fricke, Jonathan Freund, Miriam Löbbecke, and Ashley R Chadwick. «Characteristics of in-situ automated fiber placement carbon-fiber-reinforced low-melt polyaryl ether ketone laminates part 1: Manufacturing influences». In: *Journal of Composite Materials* 58.15 (Apr. 2024), pp. 1769–1787. ISSN: 1530-793X. DOI: 10.1177/00219983241244882 (cit. on p. 10).

[61] Robynne E. Murray et al. «Structural validation of a thermoplastic composite wind turbine blade with comparison to a thermoset composite blade». In: *Renewable Energy* 164 (2021), pp. 1100–1107. DOI: 10.1016/j.renene.2020.10.040 (cit. on pp. 11, 12).

[62] M. Nachtane, M. Tarfaoui, Mohamed amine Abichou, Alexandre A. Vetcher, M. Rouway, Abdeouhaed Aâmir, H. Mouadili, H. Laaouidi, and Hassan Naanani. «An Overview of the Recent Advances in Composite Materials and Artificial Intelligence for Hydrogen Storage Vessels Design». In: *Journal of Composites Science* (2023). DOI: 10.3390/jcs7030119 (cit. on pp. 11, 12, 21).

[63] H. Nishida, V. Carvelli, T. Fujii, and K. Okubo. «Thermoplastic vs. thermoset epoxy carbon textile composites». In: *IOP Conference Series: Materials Science and Engineering* 406 (2018). DOI: 10.1088/1757-899X/406/1/012043 (cit. on p. 11).

[64] Julie Pepin, Eric Lainé, Jean-Claude Grandidier, Sylvie Castagnet, Pierre Blanc-vannet, Philippe Papin, and Mathilde Weber. «Determination Of Key Parameters Responsible For Polymeric Liner Collapse In Hyperbaric Type Iv Hydrogen Storage Vessels». In: *International Journal of Hydrogen Energy* 43.33 (Aug. 2018), pp. 16386–16399. ISSN: 0360-3199. DOI: 10.1016/j.ijhydene.2018.06.177 (cit. on p. 24).

[65] Daniel L Polis, Majorie F Sovinski, Brian Harris, Dave Puckett, Charles He, and Robert Kiwak. «Cryogenic durability of a carbon fiber reinforced cyanate ester composite: degree-of-cure effect». In: *The Society for the Advancement of Material and Process Engineering (SAMPE)*. 2006 (cit. on p. 21).

[66] Weiwei Qu, Jiaxin Gao, Di Yang, Ruming He, Qian Yang, Liang Cheng, and Yinglin Ke. «Automated Fiber Placement Path Generation Method Based On Prospective Analysis Of Path Performance Under Multiple Constraints». In: *Composite Structures* 255 (Jan. 2021), p. 112940. ISSN: 0263-8223. DOI: 10.1016/j.compstruct.2020.112940 (cit. on p. 10).

[67] R.P. Reed and M. Golda. «Cryogenic Properties Of Unidirectional Composites». In: *Cryogenics* 34.11 (Jan. 1994), pp. 909–928. DOI: 10.1016/0011-2275(94)90077-9 (cit. on pp. 14, 15, 17, 18, 32).

[68] Jerad Stack Rick Dalgarno. «SM1933 - Introduction to Composite Materials». In: *AutoDesk University 2013* (2013) (cit. on p. 9).

[69] H.S. Roh, T.Q. Hua, and R.K. Ahluwalia. «Optimization Of Carbon Fiber Usage In Type 4 Hydrogen Storage Tanks For Fuel Cell Automobiles». In: *International Journal of Hydrogen Energy* 38.29 (Sept. 2013), pp. 12795–12802. ISSN: 0360-3199. DOI: 10.1016/j.ijhydene.2013.07.016 (cit. on p. 24).

[70] F. Rueda, J.P. Torres, M. Machado, P.M. Frontini, and J.L. Otegui. «External Pressure Induced Buckling Collapse Of High Density Polyethylene (hdpe) Liners: Fem Modeling And Predictions». In: *Thin-Walled Structures* 96 (Nov. 2015), pp. 56–63. ISSN: 0263-8231. DOI: 10.1016/j.tws.2015.04.035 (cit. on p. 24).

[71] Zsombor Sápi and Richard Butler. «Properties Of Cryogenic And Low Temperature Composite Materials – A Review». In: *Cryogenics* 111 (Oct. 2020), p. 103190. DOI: 10.1016/j.cryogenics.2020.103190 (cit. on pp. 12, 14, 32).

[72] Louis Schlapbach. «Hydrogen-Storage Materials For Mobile Applications». In: *nature* 414.6861 (2001), pp. 353–358 (cit. on p. 1).

[73] J.B Schutz. «Properties Of Composite Materials For Cryogenic Applications». In: *Cryogenics* 38.1 (Jan. 1998), pp. 3–12. DOI: 10.1016/s0011-2275(97)00102-1 (cit. on p. 32).

[74] S SHERIF. «Liquid hydrogen: Potential, problems, and a proposed research program». In: *International Journal of Hydrogen Energy* 22.7 (July 1997), pp. 683–688. ISSN: 0360-3199. DOI: 10.1016/s0360-3199(96)00201-7 (cit. on p. 8).

[75] S.A. Sherif, Frano Barbir, and T.N. Veziroglu. «Towards a Hydrogen Economy». In: *The Electricity Journal* 18.6 (July 2005), pp. 62–76. ISSN: 1040-6190. DOI: 10.1016/j.tej.2005.06.003 (cit. on p. 8).

[76] S Sumith and R Ramesh Kumar. «Thermo-Structural Analysis Of Cryogenic Tanks With Common Bulkhead Configuration». In: *Proceedings of the Institution of Mechanical Engineers, Part G: Journal of Aerospace Engineering* 236.5 (June 2021), pp. 900–909. ISSN: 2041-3025. DOI: 10.1177/09544100211024789 (cit. on pp. 21, 24).

[77] Eduardo Szpoganicz, Fabian Hübner, Uwe Beier, Matthias Geistbeck, and Holger Ruckdäschel. «The effect of prepreg ply thickness in carbon fiber reinforced composites on intralaminar toughness and shear strength in cryogenic environments for liquid hydrogen storage tanks». In: *Composites Part B: Engineering* 292 (Mar. 2025), p. 112077. ISSN: 1359-8368. DOI: 10.1016/j.compositesb.2024.112077 (cit. on p. 22).

[78] Klaus D. Timmerhaus. «Cryogenic Process Engineering». In: *Encyclopedia of Physical Science and Technology*. Elsevier, 2003, pp. 13–36. ISBN: 9780122274107. DOI: 10.1016/b0-12-227410-5/00156-3 (cit. on p. 8).

[79] John F. Timmerman, Brian S. Hayes, and James C. Seferis. «Cryogenic Microcracking Of Carbon Fiber/epoxy Composites: Influences Of Fiber-Matrix Adhesion». In: *Journal of Composite Materials* 37.21 (Nov. 2003), pp. 1939–1950. ISSN: 1530-793X. DOI: 10.1177/002199803036281 (cit. on pp. 12, 19, 22).

[80] Giordano Tomassetti, Renato Barboni, and Manuel de Benedetti. «Optimisation Methodology For Cryotanks». In: *Computers & Structures* 83.28–30 (Nov. 2005), pp. 2293–2305. ISSN: 0045-7949. DOI: 10.1016/j.compstruc.2005.03.034 (cit. on pp. 24, 30).

[81] Muhammad R. Usman. «Hydrogen Storage Methods: Review And Current Status». In: *Renewable and Sustainable Energy Reviews* 167 (Oct. 2022), p. 112743. ISSN: 1364-0321. DOI: 10.1016/j.rser.2022.112743 (cit. on pp. 4–6).

[82] I. M. Ward and J. Sweeney. *Mechanical Properties of Solid Polymers: Third Edition*. Wiley, Oct. 2012. ISBN: 9781119967125. DOI: 10.1002/9781119967125 (cit. on p. 12).

[83] Weiqiang Xu, Qianqian Li, and Minjie Huang. «Design And Analysis Of Liquid Hydrogen Storage Tank For High-Altitude Long-Endurance Remotely-Operated Aircraft». In: *International Journal of Hydrogen Energy* 40 (2015), pp. 16578–16586. DOI: 10.1016/J.IJHYDENE.2015.09.028. URL: https://consensus.app/papers/design-analysis-liquid-hydrogen-storage-tank-xu/84ca219417ac5fe9a9c154f6b3e5556b/ (cit. on p. 30).

[84] O. Yano and H. Yamaoka. «Cryogenic Properties Of Polymers». In: (1995). DOI: 10.1016/0079-6700(95)00003-X. URL: https://www.semanticscholar.org/paper/2a7e88924887071426a77a2ceaed0777721f4526 (cit. on p. 16).

[85] Fan Zhang, Pengcheng Zhao, Meng Niu, and Jon Maddy. «The Survey Of Key Technologies In Hydrogen Energy Storage». In: *International Journal of Hydrogen Energy* 41.33 (Sept. 2016), pp. 14535–14552. ISSN: 0360-3199. DOI: 10.1016/j.ijhydene.2016.05.293 (cit. on pp. 1, 4).

[86] Ming Zhang, Hong Lv, Huairong Kang, Wei Zhou, and Cunman Zhang. «A Literature Review Of Failure Prediction And Analysis Methods For Composite High-Pressure Hydrogen Storage Tanks». In: *International Journal of Hydrogen Energy* 44.47 (Oct. 2019), pp. 25777–25799. ISSN: 0360-3199. DOI: 10.1016/j.ijhydene.2019.08.001 (cit. on pp. 20, 21, 24).

[87] Yinnan Zhang, Fujun Xu, Chuyang Zhang, Junjie Wang, Zhemin Jia, David Hui, and Yiping Qiu. «Tensile and interfacial properties of polyacrylonitrile-based carbon fiber after different cryogenic treated condition». In: *Composites Part B: Engineering* 99 (Aug. 2016), pp. 358–365. ISSN: 1359-8368. DOI: 10.1016/j.compositesb.2016.05.056 (cit. on p. 13).

[88] Jinyang Zheng, Xianxin Liu, Ping Xu, Pengfei Liu, Yongzhi Zhao, and Jian Yang. «Development Of High Pressure Gaseous Hydrogen Storage Technologies». In: *International Journal of Hydrogen Energy* 37.1 (Jan. 2012), pp. 1048–1057. ISSN: 0360-3199. DOI: 10.1016/j.ijhydene.2011.02.125 (cit. on pp. 1, 4, 5).